SIAM Review
Vol. 48, No. 3, pp. 439–483





# Recent Developments in the Modeling, Analysis, and Numerics of Ferromagnetism*

Martin Kružík†
Andreas Prohl‡

**Abstract.** Micromagnetics is a continuum variational theory describing magnetization patterns in ferromagnetic media. Its multiscale nature due to different inherent spatiotemporal physical and geometric scales, together with nonlocal phenomena and a nonconvex side-constraint, leads to rich behavior and pattern formation. This variety of effects is also the reason for severe problems in analysis, model validation, reductions, and numerics, which have only recently been accessed and are reviewed in this work.

**Key words.** ferromagnet, Landau–Lifshitz, Landau–Lifshitz–Gilbert, mesoscopic, microscopic, harmonic map, nonconvexity, relaxation, numerics

**AMS subject classifications.** 49K20, 65K10, 65M12, 65M15, 65N50

**DOI.** 10.1137/S0036144504446187

## 1. Ferromagnetism: A Multiscale Problem.

Magnetic properties of materials have been known for more than a thousand years. About a thousand years ago, Chinese sailors started to use compasses. Even at the beginning of the 19th century, electric and magnetic effects were considered to be two independent physical phenomena. In 1820 Oersted proved that an electric current can influence a compass needle. Ampère and Faraday explained this behavior and laid the foundation for the unified theory of electrodynamics, which was developed by Maxwell. Since then, permanent magnets have found many applications in energy transformation and data storage devices. In microphones and electric generators they transform the mechanical energy of a membrane or a rotor into electric energy. In loudspeakers and motors the electric energy is transformed back into mechanical energy. Around 1900, Poulsen was the first to record an acoustic signal on a ferromagnetic wire, thus opening wide the door to applications of magnetic recording. The invention of computers has brought about the need for large data storage on easy-to-handle media. This has led to the fast development of magnetic tapes and floppy disks as well as magnetic hard disks. In general, magnetic media consist of elements that each store a single bit. The data-

*Received by the editors October 12, 2004; accepted for publication (in revised form) May 15, 2005; published electronically August 1, 2006.
http://www.siam.org/journals/sirev/48-3/44618.html

†Institute of Information Theory and Automation, Academy of Sciences of the Czech Republic, Pod vodárenskou věží 4, CZ-182 08 Praha 8, Czech Republic, and Faculty of Civil Engineering, Czech Technical University, Thákurova 7, CZ-160 00 Praha 6, Czech Republic (kruzik@utia.cas.cz). The work of this author was supported by GA AV ČR grant IAA 1075402, EU grant MRTN-CT-2004-505226 "MULTIMAT," and grant VZ6840770021 (MŠMT ČR).

‡Mathematisches Institut der Universität Tübingen, Auf der Morgenstelle 10, D-72076 Tübingen, Germany (prohl@na.uni-tuebingen.de).

writing speed is constrained by the magnetization switching time. Therefore, a deeper understanding of magnetization processes and mechanisms is important for the optimal design of magnetic recording media. Ferromagnetic models and simulations can quickly and cheaply provide reliable information that is experimentally inaccessible.

Because of various applications, ferromagnetism has become a huge field that is quickly breaking through research barriers. In this survey, we touch on some recent topics, mostly in the fields of mathematical analysis and numerics. Many others are important in the physical community, for example, thermally activated switching, device design, magnetoresistant materials, and development/benchmarking of numerical software for micromagnetic calculations [46, 34, 14]. Giant magnetoresistant materials find applications in sensors detecting a magnetic field and the presence and/or motion of iron-containing objects; another application is advanced shock absorbers. The development of both reliable and efficient software for simulation is a major challenge for numerical mathematicians and computer scientists. As will be pointed out below, both requirements are hard to meet in the construction of numerical methods, and benchmarking of corresponding codes helps to compare existing methods.

The basic idea of micromagnetics is to neglect a quantum-physical description of matter by ignoring its atomic nature and looking at it through the eyes of continuum physics. Such a theory started with Landau and Lifshitz [73], who in 1935 calculated the structure of a domain wall between two adjacent antiparallel domains. Later on, William F. Brown Jr. [18] developed a theory called micromagnetism. The basic difference from the magnetic domain theory is that one does not describe the shape of a domain in advance and then calculate an optimal magnetic structure but optimizes the domain shape.

The theory of rigid ferromagnetic bodies [18, 73] assumes that a magnetization $m : \omega \to \mathbb{R}^n$, which describes the state of a body $\omega \subset \mathbb{R}^n$, $n = 2, 3$, is subject to the Heisenberg–Weiss constraint, i.e., has a given (in general, temperature-dependent) magnitude

$$|\, m \,| = M_{\rm s} \quad \text{almost everywhere (a.e.) in } \omega \,,$$

where $M_{\rm s} > 0$ is the saturation magnetization. The Helmholtz free energy of a rigid ferromagnetic body $\omega \subset \mathbb{R}^n$ consists of three parts. The first part is the exchange energy, $\alpha \int_\omega |\nabla m|^2 \,{\rm d}x$, $\alpha > 0$, which penalizes spatial changes in $m$ and determines the finest characteristic length scale. The second part is the anisotropy energy, $\int_\omega \varphi(m) \,{\rm d}x$, related to crystallographic properties of the ferromagnet. A typical $\varphi : \mathbb{R}^n \to \mathbb{R}^* = \mathbb{R} \cup \{+\infty\}$ is a nonnegative function vanishing only at a few isolated points on $S^{n-1}$ determining directions of easy magnetization, e.g., at two points for uniaxial materials or at six (or eight) for cubic ones. Throughout the paper we will assume that $\varphi$ is a restriction of a nonnegative, even function $\tilde\varphi \in C^\infty(\mathbb{R}^n)$ to $S^{n-1} = \{s \in \mathbb{R}^n; |s| = M_{\rm s}\}$, extended by $+\infty$ out of $S^{n-1}$, i.e., $\varphi(A) = \tilde\varphi(A)$ for $A \in S^{n-1}$ and $\varphi(A) = +\infty$ if $A \notin S^{n-1}$. The third contribution of the Helmholtz energy is the magnetostatic energy, $\frac{1}{2} \int_{\mathbb{R}^n} |\nabla u|^2 \,{\rm d}x$, which comes from the stray field $-\nabla u$ governed by

$$\operatorname{div}\big( -\mu_0 \nabla u + m\chi_\omega \big) = 0 \quad \text{in } \mathbb{R}^n \,, \tag{1.1}$$

where $\chi_\omega : \mathbb{R}^n \to \{0, 1\}$ is the characteristic function of $\omega$ and $\mu_0$ is the vacuum permeability. The stray field energy thus penalizes non–divergence-free magnetization vectors. Altogether, the Helmholtz energy has the form

$$\alpha \int_\omega |\, \nabla m \,|^2 \,{\rm d}x + \int_\omega \varphi(m) \,{\rm d}x + \frac{1}{2} \int_{\mathbb{R}^n} |\nabla u|^2 \,{\rm d}x \,. \tag{1.2}$$

If the ferromagnetic specimen is exposed to some external magnetic field $H = H(x)$, Zeeman's energy of interactions between this field and the magnetization vectors equals $-\int_\omega \langle H, m\rangle_{\mathbb{R}^n}\,\mathrm{d}x$. Obviously, minimizing Zeeman's energy accounts for aligning $m$ with $H$. The standard weak formulation of (1.1) implies that the stray field energy can be equivalently expressed as

$$\frac{\mu_0}{2}\int_{\mathbb{R}^n} |\,\nabla u\,|^2\,\mathrm{d}x = \frac{1}{2}\int_\omega \langle m, \nabla u\rangle_{\mathbb{R}^n}\,\mathrm{d}x\,, \tag{1.3}$$

which is more convenient since only the integration over $\omega$ is involved.

REMARK 1.1. *Suppose $\omega = \mathbb{R}^2 \times (0,\delta)$ for $\delta > 0$. The classical formulation for* (1.1) *reads*

$$\mu_0 \Delta u = \begin{cases} \operatorname{div} m & \text{in } \mathbb{R}^2 \times (0,\delta), \\ 0 & \text{in } \mathbb{R}^2 \times \big[(-\infty,0)\cup(\delta,\infty)\big], \end{cases}$$
$$[u] = 0 \quad \text{and} \quad \mu_0 \left[\frac{\partial u}{\partial x_3}\right] = \mp m_3 \text{ on } \mathbb{R}^2 \times \{0,\delta\}\,,$$

*where $[\cdot]$ denotes the jump across the boundary of the sample. This implies that there are two sources of stray field, given by the volume charge density $-\operatorname{div} m$ in $\mathbb{R}^2\times(0,\delta)$ and the surface charge density $\pm m_3$ on $\mathbb{R}^2\times\{0,\delta\}$.*

By accounting for these mechanisms, we can write the Landau energy of the ferromagnet $\omega$ for $M_s = 1$ and values $\alpha \geq 0$ as

$$\mathcal{E}_\alpha(m) = \alpha\int_\omega |\,\nabla m\,|^2\,\mathrm{d}x + \int_\omega \varphi(m)\,\mathrm{d}x + \frac{1}{2}\int_{\mathbb{R}^n} |\,\nabla u\,|^2\,\mathrm{d}x - \int_\omega \langle H, m\rangle_{\mathbb{R}^n}\,\mathrm{d}x\,, \tag{1.4}$$

together with (1.3), for $\mu_0 \equiv 1$. According to Landau's model, observed magnetization patterns correspond to minimizers of this energy; as Brown [18] outlined, minimizers to (1.4) solve the torque equation that involves the effective field $H_{\text{eff}} = -D\mathcal{E}_\alpha(m)$, i.e.,

$$m \times H_{\text{eff}} = 0\,.$$

In the following, we mainly focus on uniaxial materials (e.g., cobalt) that penalize magnetizations that do not align with the easy axis $e \in \mathbb{R}^n$, i.e., $\varphi(m) = \beta\,|\,\langle m, e_\perp\rangle\,|^2$, $\beta \geq 0$. Media with a low value of $\beta$ are called soft, because the magnetization is easy to rotate. The multiscale nature of intrinsic $\alpha, \beta \geq 0$ and geometric scales of the variational problem formulated as the minimization of (1.4), together with the nonconvex (Heisenberg–Weiss) constraint and nonlocality (stray field contribution), leads to rich behavior and pattern formation on intermediate scales.

Historically, physical investigations in micromagnetism initially concentrated on static magnetization configurations observed in bulk specimens up to submicrometer size. Early observations of ferromagnetic domains in iron crystals around 1956 revealed both the fascinating intricacies of domain patterns and, nevertheless, their strong geometric nature; decades later, the realm of domain patterns has been enriched by numerous observations, which, on many occasions, have stressed the multiscale nature of their arrangements. One main concept is the competition of the wall energy and the energy arising from surface magnetic charges necessarily present in a uniformly magnetized confined specimen. For sizes above the single domain limit, only a finite number of magnetization distributions called (ground) states may be generated, depending on the field application and, more generally, the magnetic history.

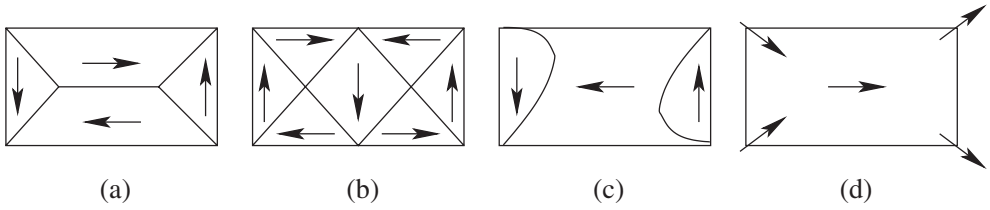


**Fig. 1.1** *Domains: Four different magnetization states in* 2:1 *aspect ratio (cubic) platelets:* (a) *"Landau,"* (b) *"Diamond,"* (c) *"S,"* (d) *"Flower."*

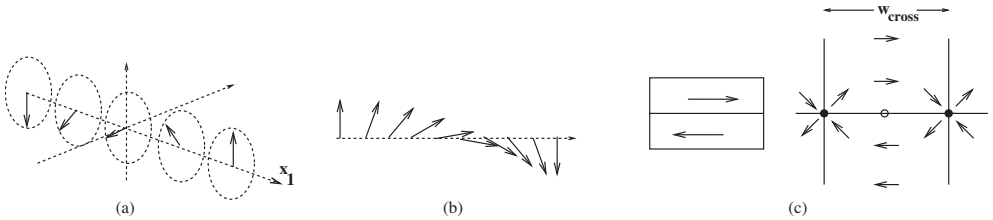


**Fig. 1.2** *Domain walls:* (a) *Bloch wall,* (b) *Néel wall (simple wall),* (c) *cross-tie wall (complex wall): mesoscopic (left) and microscopic (right) structure.*

Observation 1.1. *Computations for Permalloy-type materials of size* $2 \times 1\ \mu m^2$ *for a* 20 *nm thickness indicate that two flux-closure ground states ("Landau" and "Diamond") have noticeably lower energies than the high-remanence states ("S" and "Flower"); see Figure* 1.1. *Intricacies also soon arise when allowing for the existence of complex walls such as cross-tie walls (see Figure* 1.2*), which are stable wall structures in continuous Permalloy films in the* 20 *nm thickness range; for such thicknesses, accurate computations of wall energies prove essential when attempting to define the hierarchy of flux-closure states. As the size decreases to* $0.5 \times 0.25\ \mu m^2$ *and the thickness to* 10 *nm, however, the Landau state becomes the lowest-energy state, soon followed, however, by the S state, the Diamond state, and, last, the Flower state. Clearly, the Flower state is closest to a uniformly magnetized state. However, the S state appears only marginally metastable and, besides, may easily be generated through the application of the saturating field at an angle to the horizontal axis. These considerations show that submicron dimensions need to be reached before high-remanence states, i.e., the states proper to memory applications, for instance, may be considered sufficiently stable. As is easily guessed from purely magnetostatic arguments, platelet properties exhibit a strong shape dependence, leading to configurational anisotropy for platelets with high symmetry, such as squares, triangles, and pentagons, where the conventional shape anisotropy vanishes.*

Domains of ground states are separated by interfaces called walls, which exhibit internal structure and are of order $\mathcal{O}(\sqrt{\alpha/\beta})$ thick, which typically amounts to a few dozen nanometers. According to their structure, different simple walls (Bloch, Néel walls) and complex walls (cross-tie walls, asymmetric Bloch and Néel walls) are known [14, 55]; see Figure 1.2. Structures of even smaller size are vortices in thin films and Bloch lines in bulk materials. Vortices appear as embedded structures in cross-tie walls or at the intersection of domain walls, leading to a nontrivial topological arrangement of the magnetization field. Their dynamics is highly nontrivial and at the present time poorly understood.

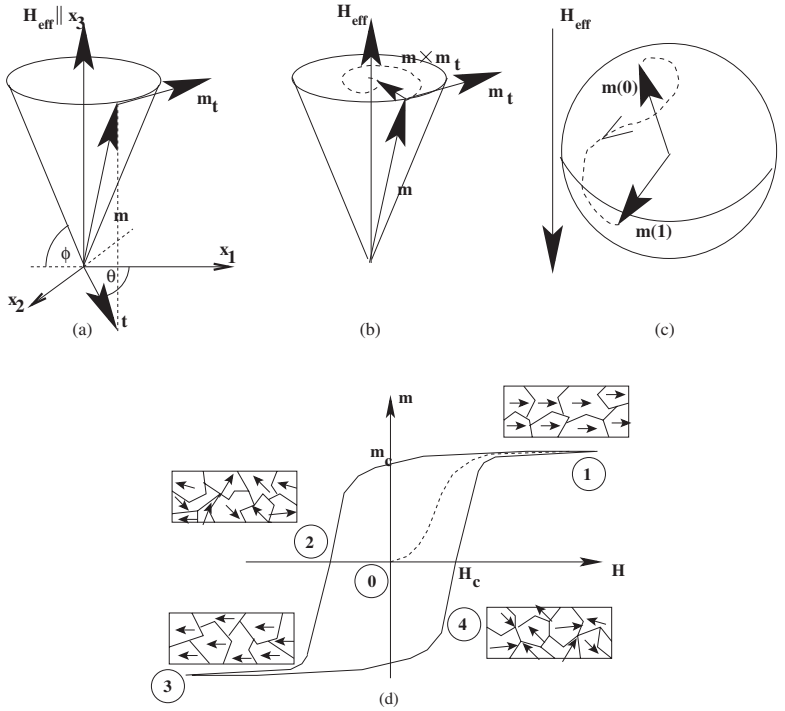


**Fig. 1.3** *Magnetization precession* (a) *without damping;* (b) *with damping;* (c) *switching/reversal process;* (d) *virgin curve and hysteresis loop.*

OBSERVATION 1.2. *Domain walls are transition layers between magnetic domains which possess a rich internal structure. The simplest among them are* 180° *plane walls separating two domains of opposite direction: The Bloch wall (Figure* 1.2(a)*) occurs in bulk materials, where transition proceeds perpendicular to the transition axis; the main feature of this scenario is avoidance of magnetic volume charges, i.e.,* $\operatorname{div} m = 0$. *If rotation proceeds in the plane spanned by the transition axis and end states, this layer is referred to as a Néel wall (Figure* 1.2(b)*). It is the dominating type of wall in very thin films, where Bloch walls would create significant surface charges; Néel walls completely avoid surface charges, but are a source of (small) out-of-plane magnetization as well as volume charges. In moderately thick films the most common wall type is the cross-tie wall (Figure* 1.2(c)*). This energetically more favorable composite wall replaces the* 180° *Néel wall by a pattern of a main Néel-wall segment (orientationally favored by the anisotropy energy) and perpendicular short Néel wall segments (the cross-ties) periodically lining up at a new scale* $w_{\text{cross}}$. *All Néel walls in the cross-tie pattern show transition angles of* 90° *or less.*

Besides multiple spatial scales, micromagnetism shows a rich variety of complex nonstationary phenomena; historically, the study of magnetization reversal processes in the quasi-static regime came first, where the spin configuration is observed following the magnetization loop of an applied field. In contrast to static and quasi-static investigations, the wide variety of dynamic properties of magnetic elements can only be understood by using precessional motion to explain spin dynamics and switching dynamics at speeds of pico- or even femptosecond time scales; cf. Figure 1.3. Mesoscopic changes during a corresponding experiment may be displayed by hysteresis

loops, which plot the average magnetization at the steady state as a function of the applied field strength; see Figures 1.3(d) and 3.5.

OBSERVATION 1.3. *If we apply an external magnetic field to a (fully demagnetized) ferromagnet, the ferromagnet absorbs part of the external field by growing aligned domains until saturation is reached. Even when the external field is removed, the magnet will retain some field (remanence): it has become magnetized; see, e.g., Figure* 1.3(d). *When the external field is cycled in time, the corresponding magnetization of the magnet traces a hysteresis loop. In many cases we observe that the dependence of the magnetization on the external field is rate independent, which means that it is invariant to any increasing time homeomorphism. The property of rate-independence is named after Truesdell and Noll* [105]. *Following Visintin* [107], *we define hysteresis as a rate-independent memory effect. Actually, typical memory effects in ferromagnetism are not purely rate-independent, since hysteresis is coupled with viscous effects. However, rate-independence prevails provided that the evolution is not too fast. See, e.g.,* [108] *for a version of the Landau–Lifshitz equation accounting for rate-independent effects.*

The interest in magnetic materials gained a completely new and unforeseen momentum when growth and lithographic patterning methods, known from the field of semiconductors, were applied to magnetic material classes, which resulted in the discovery of a number of fascinating properties: starting with the growth of artificial layered magnetic materials, with layer thicknesses on the atomic scale, the giant magnetoresistance effect and quantum-size effects in the electronic and magneto-optical properties have been observed. These studies pose new questions, for example, about the magnetization reversal process induced by external field pulses of short duration, the role of precessional damping, nonstationary magnetization patterns, and magnetic anisotropies, as well as the influence of the geometric shape and size of the ferromagnetic specimen on this field-induced reversal process. For example, the dynamics of small magnetic elements is expected to differ from that measured in (single-layer) magnetic films due to different relative roles played by the exchange and anisotropy energy contributions driving the evolution.

Mathematical models in ferromagnetism focus on certain ranges of spatiotemporal scales to describe corresponding magnetic phenomena. The following levels of description may be distinguished (freely after [96]):

1. *Atomic level*: Statistical physics is used to describe single magnetic spin moments and their interaction in a finite ensemble.
2. *Microscopic level*: Continuum physics is used to describe the problem. Usually scales of about 1 $\mu$m down to dozens of nanometers can be treated. The commonly used models at this level are the nonconvex, nonlocal Landau–Lifshitz energy functional and the strongly coupled, degenerated quasi-linear parabolic Landau–Lifshitz–Gilbert (LLG) equation, e.g., to predict the structure and evolution of domains and walls. See sections 2.2 and 3.2.
3. *Mesoscopic level*: Characteristic microscopic length scales of the magnetic material are ignored in a large-body limit to model specimens of engineering interest. The averaged magnetization is a global minimizer of a degenerate convex, nonlocal, asymptotic variational problem, and the microstructure is described by volume fractions of particular magnetic poles. Further applications include the description of inhomogeneous magnetization in bulk specimens up to millimeter size and microstructure in single crystals; cf. sections 2.3 and 3.3.

4. *Macroscopic level*: Information about microstructure is suppressed, and phenomenological constitutive laws describe the evolution of gross magnetization during external loading. This simplification is a compromise with level 3, with limited computational resources needed for advanced applications.

Over the last decades, considerable effort has been made to study mathematically related stationary and nonstationary models for different regimes of scales: next to well-posedness and further characterizations of solutions (e.g., study of singularity sets, asymptotics), models have been validated through theoretical predictions (e.g., prediction of phenomena, scaling laws, reduced models). Mathematical difficulties inherent to these models (e.g., nonconvexity, nonlocality, strong nonlinearities, degeneracies, measure-valued solutions), as well as multiple scales inherent to solutions, also make the construction of efficient, convergent numerical schemes a nontrivial task. The goal of this article is to survey the recent status of mathematical modeling, analysis, and numerics of ferromagnetism as it appears to the authors. In the following we will use standard Lebesgue spaces $L^p$, Sobolev spaces $H^1$, and spaces of bounded variations $BV$.

**2. Stationary Models: Multiscale Properties of Ground-State Magnetizations.** The variational theory of Landau and Lifshitz [73] describes magnetizations and corresponding domain-wall structures inside a ferromagnetic body $\omega \subset \mathbb{R}^n$ as minima of the energy functional

$$\mathcal{E}_\alpha : \mathcal{A} \cap H^1(\omega, \mathbb{R}^n) \to \mathbb{R}\,, \qquad \mathcal{A} = \Big\{ \phi \in L^2(\omega, \mathbb{R}^n) \Big| \; |\,\phi\,| = 1 \text{ a.e. in } \omega \Big\}\,,$$

given in (1.4). The anisotropy density $\varphi \geq 0$ is zero in the case $m \parallel e_i \in \mathbb{R}^n$ for $i \in I$, with some index set $I$, and positive otherwise. Vectors $e_i \in \mathbb{R}^n$ are referred to as easy axes. The model describes multiscale domain branching and structured domain walls by competition of local and nonlocal energy contributions in (1.4), which are observed in experiments for ferromagnets of different anisotropic materials (e.g., uniaxial, where $\#I = 1$, or cubic, where $\#I = 3$ or 4). For example,

1. multiscale branching near surfaces in uniaxial materials is explained by reduced magnetostatic energy contributions that only depend on the domain width of the last branching generation at the boundary $\partial\omega$;
2. the geometric structure of domain walls may be explained by accounting for competing effects due to all involved energy contributions.

As can be deduced from harmonic mapping theory [56, 101], solutions $m \in \mathcal{A}$ to (1.4) exist and may be characterized in terms of regularity provided that $\alpha > 0$; a nontrivial task due to the nonconvex side-constraint is to construct a convergent numerical scheme for restricted (finite-element) functions to approximate solutions to (1.4), (1.1); see section 2.2.

The model of Landau and Lifshitz describes equilibria for ferromagnetic bodies on a microscopic level; in contrast, mesoscopic models are in demand for practical applications to describe averaged magnetizations for bulk specimens typically of millimeter size. This goal motivates a reduced version of (1.4), which is obtained by deleting the exchange energy contribution, i.e., if $\alpha = 0$,

$$\mathcal{E}_0 : \mathcal{A} \to \mathbb{R}\,, \tag{2.1}$$

allowing for infinite variations (microstructure) in space. In fact, $\mathcal{E}_0$ is a good approximation of $\mathcal{E}_\alpha$ for large bodies $\omega$, as shown in [36]. Generic oscillatory behavior

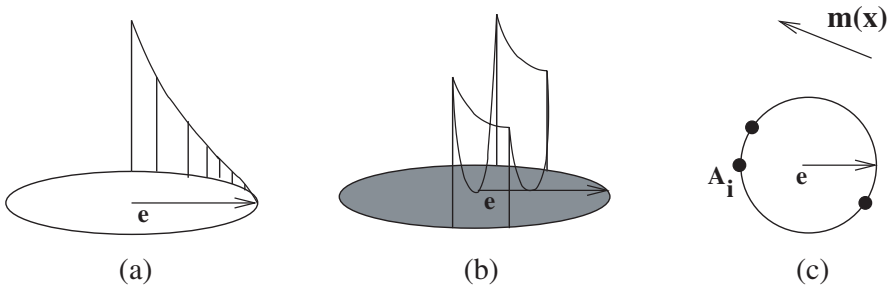


**Fig. 2.1** *Minimization of Landau–Lifshitz energy:* (a) *direct minimization:* $m(x) \in S^{n-1}$*;* (b) *convexification:* $|\,m(x)\,| \le 1$*;* (c) *Young-measure relaxation:* $\nu_x = \sum_{i=1}^{3} \alpha_i \delta_{A_i}$ *(example).*

of minimizing sequences of $\mathcal{E}_0$ typically leads to nonexistence of a minimizer, and a relaxation of $\mathcal{E}_0$ is desirable; cf. Figure 2.1. One proper mathematical tool to describe minimizing magnetization configurations of a relaxed version of this energy functional is the Young-measure solution. We refer to [86, 94] for a detailed exposition of Young measures and applications. The Young measure $\nu = \{\nu_x\}_{x\in\omega} \in L^\infty_{\rm w}\big(\omega, \mathcal{M}(S^{n-1})\big) = (L^1(\omega; C(S^{n-1})))^*$, where $\|\nu_x\| = 1$ for almost all $x \in \omega$ and $\mathcal{M}(S^{n-1})$ denotes measures supported on $S^{n-1}$. Here, the subscript "w" means weakly measurable maps, i.e., $x \mapsto \int_{S^{n-1}} f(A)\nu_x(\mathrm{d}A)$ is measurable for any $f$ continuous on $S^{n-1}$. Young measures encode (oscillatory) microstructures and also allow for calculation of averaged magnetizations $m(x) = \int_{S^{n-1}} A\nu_x(\mathrm{d}A)$, with $|\,m(x)\,| \le 1$ for almost every $x \in \omega$. The relaxation of $\mathcal{E}_0 : \mathcal{A} \to \mathbb{R}$ consists in setting up a new functional $\overline{\mathcal{E}_0}$ and its admissible set $\overline{\mathcal{A}}$, where

$$\overline{\mathcal{A}} = \Big\{ \nu = \{\nu_x\}_{x\in\omega} \Big|\ \operatorname{supp}\nu_x = S^{n-1},\ x \mapsto \nu_x \text{ weakly measurable} \Big\}.$$

We then ask for minima of $\overline{\mathcal{E}_0} : \overline{\mathcal{A}} \times L^2(\omega;\mathbb{R}^n) \to \mathbb{R}$, where

$$\overline{\mathcal{E}_0}(\nu) := \int_\omega \int_{S^{n-1}} \varphi(A)\nu_x(\mathrm{d}A)\,\mathrm{d}x + \frac{1}{2}\int_{\mathbb{R}^n} |\,\nabla u\,|^2\,\mathrm{d}x - \int_\omega \langle H, m\rangle_{\mathbb{R}^n}\,\mathrm{d}x\,, \tag{2.2}$$

$$\text{subject to} \qquad m(x) = \int_{S^{n-1}} A\nu_x(\mathrm{d}A) \quad \text{and} \quad \Delta u = \operatorname{div}(\chi_\omega m) \quad \text{in } \mathbb{R}^n\,.$$

The minimizations of (2.1) and (2.2) are linked together by standard relaxation theory, i.e., (i) $\inf_{\mathcal{A}} \mathcal{E}_0 = \min_{\overline{\mathcal{A}}} \overline{\mathcal{E}_0}$, (ii) minimizers of $\overline{\mathcal{E}_0}$ are weak limits of minimizing (sub)sequences of $\mathcal{E}_0$, and (iii) minimizing (sub)sequences of $\mathcal{E}_0$ weakly star tend to minimizers of $\overline{\mathcal{E}_0}$; see also Figure 2.1. It is nontrivial to ensure that the magnetostatic energy in (2.2) evaluated along a minimizing sequence of (1.4) converges to the weak limit of a minimizing sequence for (1.4). The basic tool to show this is the div-curl lemma [84, 104]. Indeed, as $m_k \to m$ weakly* in $L^\infty(\omega,\mathbb{R}^n)$, $\nabla u_k \to \nabla u$ weakly in $L^2(\mathbb{R}^n,\mathbb{R}^n)$, and since $\{\nabla u_k\}$ is curl free it is sufficient to show that $\{\operatorname{div} m_k\}$ is compact in $H^{-1}_{\rm loc}(\mathbb{R}^n)$. Then we have

$$\int_\omega \langle m_k, \nabla u_k\rangle_{\mathbb{R}^n}\,\mathrm{d}x \to \int_\omega \langle m, \nabla u\rangle_{\mathbb{R}^n}\,\mathrm{d}x\,.$$

Therefore, it would be natural to define measure-valued magnetization as a Young measure supported on $S^{n-1}$ which is generated by sequences $\{m_k\}$, where $\{\operatorname{div} m_k\} \Subset$

$H^{-1}_{\rm loc}(\mathbb{R}^n)$. This would impose an additional constraint on the Young measure. Fortunately, as shown in [36, 85, 86], any Young measure supported on $S^{n-1}$ can be generated by a sequence satisfying the compactness constraint.

We now briefly explain the construction in $\mathbb{R}^2$ which was already used in [36]. Suppose that $A_1, A_2, A_3 \in S^1$ support the Young-measure solution $\nu = \vartheta\mu\delta_{A_1} + \vartheta(1-\mu)\delta_{A_2} + (1-\vartheta)\delta_{A_3}$. (Note that $n+1$ points are sufficient in $n$ dimensions.) Any $m^k \in L^2(\omega;\mathbb{R}^2)$ can be approximated by piecewise constant functions on $\omega$. Thus the problem turns into an approximation of a constant function on a given set $O \subset \omega$. Take $q \in \mathbb{R}^2$ such that $\langle \mu A_1 + (1-\mu)A_2 - A_3, q\rangle_{\mathbb{R}^2} = 0$ and $p \in \mathbb{R}^2$ such that $\langle A_1 - A_2, p\rangle_{\mathbb{R}^2} = 0$. This choice of $p, q$ ensures the convergence of magnetostatic energies. Define

$$\theta(t) = \begin{cases} 1 & \text{if } 0 \le t < \vartheta, \\ -1 & \text{if } \vartheta \le t < 1, \end{cases} \quad \text{and} \quad \eta(t) = \begin{cases} 1 & \text{if } 0 \le t < \mu, \\ -1 & \text{if } \mu \le t < 1, \end{cases}$$

and extend them periodically over the whole space. Then we define for $\xi, \zeta \in \mathbb{N}$

$$\mathcal{L}_{\xi\pm} = \{x \in O;\ \theta(\xi\langle x, q\rangle_{\mathbb{R}^2}) = \pm 1\}\ , \qquad \mathcal{M}_{\zeta\pm} = \{x \in O;\ \eta(\zeta\langle x, p\rangle_{\mathbb{R}^2}) = \pm 1\} \cap \mathcal{L}_{\xi+}\ .$$

Then we have

$$\tilde{m}_{\xi,\zeta}(x) = \begin{cases} A_1 & \text{if } x \in \mathcal{M}_{\zeta+}, \\ A_2 & \text{if } x \in \mathcal{M}_{\zeta-}, \\ A_3 & \text{if } x \in \mathcal{L}_{\xi-}. \end{cases}$$

Finally,

$$\tilde{m}_{\xi}(x) = \begin{cases} \mu A_1 + (1-\mu)A_2 & \text{if } x \in \mathcal{L}_{\xi+}, \\ A_3 & \text{if } x \in \mathcal{L}_{\xi-}, \end{cases}$$

with $\text{weak-lim}_{\zeta\to\infty} \tilde{m}_{\xi,\zeta} = \tilde{m}_\xi$ in $L^2(\omega;\mathbb{R}^2)$ and $\text{weak-lim}_{\xi\to\infty} \tilde{m}_\xi = m$ in $L^2(\omega;\mathbb{R}^2)$. Eventually, we get a sequence weakly approaching a constant function on $O$. We refer to [36], where it is shown that the sequence above is really minimizing. The minimizing sequence is obtained by the appropriate scaling of the picture on the right-hand side of Figure 2.2. The strip of thickness $1-\mu$ belongs to $\mathcal{L}_{\xi+}$, and the strip of thickness $\mu$ belongs to $\mathcal{L}_{\xi-}$. Similarly, strips of width $\mu$ and $1-\mu$ are subsets of $\mathcal{M}_{\zeta+}$ and $\mathcal{M}_{\zeta-}$, respectively.

Another representation of the relaxation of $\mathcal{E}_0$ uses the convex envelope $\varphi^{**}$ of $\varphi$. We recall that the convex envelope is the supremum of all convex functions not greater than $\varphi$. We remark that $\varphi^{**}$ can be explicitly calculated in particular cases. See [36] for some examples. The problem now reads as follows: Minimize

$$\tilde{\mathcal{E}}_0 : \tilde{\mathcal{A}} \to \mathbb{R}\,, \quad \tilde{\mathcal{A}} = \Big\{\phi \in L^2(\omega,\mathbb{R}^n)\Big|\ |\,\phi\,| \le 1 \text{ a.e. in } \omega\Big\}\,, \tag{2.3}$$

where

$$\tilde{\mathcal{E}}_0(m) = \int_\omega \varphi^{**}(m)\,\mathrm{d}x + \frac{1}{2}\int_{\mathbb{R}^n} |\,\nabla u\,|^2\,\mathrm{d}x - \int_\omega \langle H, m\rangle_{\mathbb{R}^n}\,\mathrm{d}x\,, \quad \Delta u = \mathrm{div}\big(\chi_\omega m\big) \quad \text{in } \mathbb{R}^n\,. \tag{2.4}$$

Minima of $\tilde{\mathcal{E}}_0$ may be characterized as solutions of corresponding Kuhn–Tucker equations: Find $(\,m, u, \lambda\,) \in L^2(\omega,\mathbb{R}^n) \times H^1(\mathbb{R}^n) \times L^2(\omega)$ such that

$$(\nabla u, \nabla w) = (m, \nabla w) \quad \forall\, w \in H^1(\mathbb{R}^n)\,, \tag{2.5}$$

$$\nabla u + D\varphi^{**}(m) + \lambda m = H \quad \text{a.e. in } \omega\,, \tag{2.6}$$

$$0 \le \lambda\,, \quad |\,m\,| \le 1\,, \quad \text{and} \quad \lambda(1 - |\,m\,|)_+ = 0 \quad \text{a.e. in } \omega\,. \tag{2.7}$$

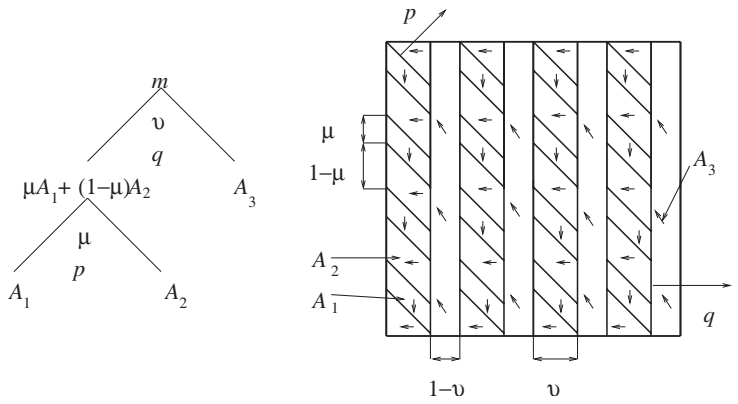


**Fig. 2.2** *Construction of a minimizing sequence on $O$.*

Here, $(s)_+ := \max\{s, 0\}$ denotes the nonnegative part, and the last condition in (2.7) states that $\lambda \neq 0$ is possible only for $|\,m\,| = 1$, as a consequence of $\lambda m \in \partial\mathfrak{Z}(m)$ for the convex characteristic functional $\mathfrak{Z} : \mathbb{R}^2 \to [0, \infty]$ defined by $\mathfrak{Z} = 0$ if $|\,m\,| \leq 1$ and $\mathfrak{Z} = \infty$ if not.

The subsequent sections survey both analytical and numerical aspects of these strategies to describe magnetization configurations on microscopic and mesoscopic levels. We begin with an interesting recent interpretation of the Landau–Lifshitz model as a limiting problem of a statistical approach. Section 2.2 discusses scaling properties of domains and walls in terms of physical ($\alpha, \beta \geq 0$) and geometric ($\ell, \delta \geq 0$) parameters, and numerics are discussed in section 2.2.1. Section 2.3 deals with Landau–Lifshitz energy without exchange energy; in particular, we evidence high complexity of algorithms in the course of direct minimization of $\mathcal{E}_0 : \mathcal{A}_h \to \mathbb{R}$ for finite-dimensional subsets $\mathcal{A}_h \subset \mathcal{A}$, which historically came first in the numerical analysis of minimizing (1.4), in section 2.3.1; in section 2.3.2, strategies to discretize the degenerate elliptic problem (2.5)–(2.7) are reviewed; in section 2.3.3, a convergent scheme using discretized Young measures to minimize the linear-quadratic problem is discussed. Section 2.4 discusses a reduced model in the thin film limit.

**2.1. Statistical Theory Derivation of the Landau–Lifshitz Model.** The statistical mechanics of a lattice spin system with a continuous order parameter is capable of describing equilibrium states of magnetic media. In relatively small-scale devices thermal fluctuations affect the behavior of magnetic domain walls, which need to be incorporated into the continuum model. Katsoulakis, Plecháč, and Tsagkarogiannis [59, 60] derived this limiting problem from statistical mechanics considerations using the large deviation theory. They considered an $n$-dimensional periodic lattice. At each side $x$ of this lattice is an order parameter $\sigma$ representing the magnetic spin moment with values on the unit sphere $S^{n-1}$.

The most probable configuration of the system is then given by the Maxwellian distribution depending on $(x, v)$, $v \in S^{n-1}$:

$$M(x, v) = \frac{1}{Z_b(x)} \exp\Big(-b\big(\varphi(v) + \langle v, \nabla\bar{u} - J * \bar{m} - H\rangle_{\mathbb{R}^n}\big)\Big).$$

Here, $J$ describes local mean field interaction in the exchange energy and $Z_b$ is the corresponding partition function with $b = (kT)^{-1}$ for $k$ the Boltzmann's constant and

$T$ the absolute temperature. Moreover, $(\bar{u}, \bar{m})$ minimize a new free energy

$$E_b(m) = \frac{1}{2}\int_{\mathbb{R}^n} |\nabla u|^2 \,\mathrm{d}x - \frac{1}{2}\int_\omega \langle J * m, m\rangle_{\mathbb{R}^n}\,\mathrm{d}x + \int_\omega a_b^*(m)\,\mathrm{d}x - \int_\omega \langle H, m\rangle_{\mathbb{R}^n}\,\mathrm{d}x\,, \tag{2.8}$$

where "*" stands for the convolution and $a_b^*$ for the Legendre–Fenchel transform of

$$a_b(p) = \beta^{-1}\log\int_{S^{n-1}} \exp\bigl(-b(\varphi(v) + \langle v, p\rangle_{\mathbb{R}^n})\bigr)\,\mathrm{d}v\,.$$

Expanding the convolution term in (2.8), one gets the finite-temperature analogy of the Landau–Lifshitz energy (1.4). An important point is that the energy (2.8) is minimized subject to the constraint $|m| \le 1$, while the Landau–Lifshitz energy is considered for $|m| = 1$. The earlier mentioned convex constraint is due to thermal fluctuations, and the Landau–Lifshitz energy can be seen as the low-temperature limit of the energy (2.8).

**2.2. The Landau–Lifshitz Energy: A Microscopic Model.** The presence of the exchange energy contribution in the energy functional (1.4) is the reason for a variety of microscopic, multiscale magnetic phenomena like domains, structured domain walls, branching of domains, and closure domains. Construction of solutions $m = \operatorname{argmin}_{\mathcal{A}\cap H^1(\omega,\mathbb{R}^n)}\mathcal{E}_\alpha(\phi)$ is by minimizing sequences $\{m_\ell\}_\ell \subset \mathcal{A}\cap H^1(\omega,\mathbb{R}^n)$, which possess weakly convergent subsequences $\{m_\ell\}_\ell \subset H^1(\omega,\mathbb{R}^n)$, whose limit $m^* \in H^1(\omega,\mathbb{R}^n)$ also satisfies $|\,m^*\,| = 1$ for almost every $x \in \omega$ by a compactness argument. Passing to the limit with respect to each energy contribution now follows by weakly lower semicontinuity properties of each involved energy contribution. Explicit solutions are only known in special cases; the next example by Landau and Lifshitz [73] is taken from [90].

EXAMPLE 2.1. *Let $\omega = \mathbb{R}^3$, $\xi_i \in \mathbb{R}^3$ be the unit vector in the $x_i$-direction, and $e = \xi_3$. Suppose $m = m(x_1)$ and $\lim_{x_1\to\pm\infty} m(x_1) = \pm\xi_3$. Then stray field contributions in the Landau–Lifshitz energy (without external field) can be computed, and hence*

$$\mathcal{E}_\alpha(m) = \int_{-\infty}^{+\infty} \alpha\,|\,m'\,|^2 - \langle m, Tm\rangle_{\mathbb{R}^3}\,\mathrm{d}x_1\,, \qquad T = \beta\,\xi_3\otimes\xi_3 - \xi_1\otimes\xi_1\,. \tag{2.9}$$

*Parameterization of $m$ using angles $(\vartheta,\iota) = (\frac{\pi}{2}-\phi, \frac{\pi}{2}-\theta) \in [0,\pi]\times[-\pi,\pi]$ (cf. Figure 1.3(a)) yields a representation*

$$m(\vartheta,\iota) = \cos(\vartheta\xi_3) + \sin\bigl(\vartheta t(\iota)\bigr)\,, \qquad t(\iota) = \sin(\iota\xi_1) + \cos(\iota\xi_2)\,,$$

*and the minimizer of (2.9) has the form*

$$\vartheta(x_1) = \arccos\left(\tanh\frac{x_1}{w}\right)\,, \qquad \iota(x_1) = 0\,,$$

*with $w = \sqrt{\alpha/\beta}$. Hence, the magnetization is nearly parallel to the easy axis at large distances from the origin, and these domains are separated by a Bloch domain wall $(-w, w)$ centered around the origin.*

For highly anisotropic, uniaxial materials, domain branching and domains of specific scales are experimentally observed multiscale phenomena which may be explained as an energy-minimizing mechanism in the context of micromagnetic theory. Figure 2.3(a) shows oscillatory patterns of magnetizations of strongly uniaxial ferromagnets along the easy axis to avoid volume charges, whereas "closure domains" are added

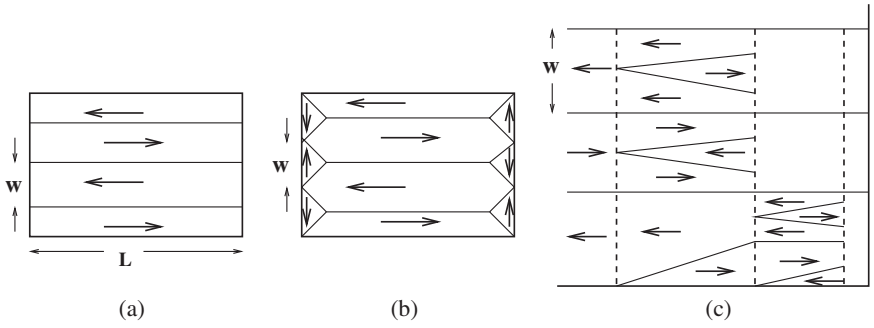


**Fig. 2.3** *Multiscale phenomena and scaling laws in a uniaxial ferromagnet:* (a) *oscillatory magnetization pattern of layer width* $w$, (b) *closure domains added to eliminate surface charges,* (c) *domain branching due to Privorotskii* [92] *(sketch).*

in Figure 2.3(b) along the boundary to avoid surface charges at the expense of small anisotropy and surface energy contributions. Finally, multiscale oscillatory structures are arranged in a complex branching pattern on surfaces perpendicular to the easy axis in the vicinity of $\partial\omega$ (see Figure 2.3(c)). In [27, 28] a simplified energy $\underline{\mathcal{E}} : \underline{\mathcal{A}} \to \mathbb{R}$ for $\underline{\mathcal{A}} = \{\phi \in BV(\omega, \mathbb{R}^n) | \, |\, \phi \,| = 1 \text{ a.e. in } \omega\}$ and $\omega = (0, \ell) \times \omega' \subset \mathbb{R}^n$ is considered, i.e.,

$$\underline{\mathcal{E}}(m) = \alpha \, |\, Dm \,|(\omega) + \beta \int_\omega m_2^2 + m_3^2 \, \mathrm{d}x + \frac{1}{2} \int_{\mathbb{R}^3} |\, \nabla u \,|^2 \, \mathrm{d}x \,,$$

to study branching and inherent scalings for strongly uniaxial materials. Here, $|\, Dm \,|$ denotes the total variation of $m$. This "wall" energy is chosen to restrict to sharp interfaces: it allows for jumps of $m$ across a surface and assigns to them an energy proportional to the jump height and surface area, neglecting possible internal wall structure (see below). In this case layers of width $w_{\min} \sim \sqrt{\alpha\ell}$ generate magnetization patterns of energy $\underline{\mathcal{E}}_{\min} \sim \sqrt{\alpha\ell}$ (Figure 2.3(a)), which may be reduced to $\underline{\mathcal{E}}_{\min} \sim \sqrt{\alpha\beta\ell}$ for $w_{\min} \sim \sqrt{(\alpha\ell)/\beta}$ by using closure domains in Figure 2.3(b) in the case $\beta < 1$. Finally, Privorotskii's branching construction [92] to balance surface and anisotropy energies of closure domains creates significantly lower energies $\sqrt[3]{\alpha^2 \ell \min\{\beta, 1\}}$ for typical bulk domain sizes $w_{\min} = \sqrt[3]{\alpha\ell^2 / \min\{\beta, 1\}}$, provided samples are sufficiently large to allow for branching structures, i.e., $\ell \gg \max\{\frac{\alpha}{\beta}, \alpha\}$ and $\sqrt[3]{\alpha\ell^2 / \min\{\beta, 1\}} \ll 1$. These scaling laws evidence the sharpness of the above branching constructions and hence detect domain branching as one essential multiscale phenomenon in micromagnetism. However, it is not clear from the energy-based arguments what are characteristic length scales in the planes $x = 0, \ell$. Also, one might imagine from Figure 2.3(a)–(c) that three-dimensional structures of uniaxial materials achieve a better scaling law—a possibility that is ruled out in [28]. Finally, it is still not clear if corresponding observations hold for the exchange energy $\alpha \, \| \, \nabla m \, \|^2$ as well, which moreover allows for internal wall structures of magnetizations.

The study of inner structures of domain walls is one of the major research topics in micromagnetism nowadays. The existence, internal structure [6, 77], stability [41], and interaction [38] of different observed simple and complex domain walls exhibiting multiple scales (Figure 1.1) may also be understood for specific ranges of material and geometric parameters by the Landau–Lifshitz energy (1.4). For thin soft ferromagnetic

films $\omega = (0,\ell)^2 \times (0,\delta)$, $\delta > 0$, and practically relevant parameter regimes, two-dimensional Néel walls are the favorite wall type, yielding to minimizing energies of magnitude $\mathcal{O}\big(\delta^2 \log^{-1}(\frac{\delta}{\alpha^2})\big)$; cf. section 2.4 and [38, 37]. These theoretical studies of Néel walls support experimental observations in thin samples, according to which they consist of a small core with fast-varying rotation and two far-reaching, logarithmically decaying tails. Melcher [77] has given a more detailed analysis providing corresponding scaling laws of the pointwise behavior of the one-dimensional Néel wall if confined by anisotropy energy. Understanding the interaction of such walls with one another or with the boundary using Landau–Lifshitz energy is a subject of current research. Another recent result [41] establishes the stability of one-dimensional Néel walls in thin films under two-dimensional perturbations; derived scaling laws for minimizing energies also evidence why energetically favorable cross-tie walls in moderately thick films are replaced by Néel walls as the thickness of the sample decreases. These results provide the basis for understanding better structures and scalings of more complex walls, such as, e.g., cross-tie walls, which are composed of Néel walls (cf. Figure 1.1(c)); we refer to [38] for further discussion.

**2.2.1. Algorithms to Minimize the Landau–Lifshitz Energy.** If restricted to the first energy contribution in (1.4), stationary points of (1.4) are called harmonic maps, which are by now well understood with respect to properties like existence, nonuniqueness, regularity, and singularities of both minimizing and nonminimizing harmonic maps. Numerically, it is challenging to meet the energy decay property $\mathcal{E}_\alpha(m_h^j) \le \mathcal{E}_\alpha(m_h^{j-1})$, $j \ge 1$, with the nonconvex side-constraint $|\, m_h^j \,| = 1$ in an iterative context $j \ge 0$. Guided by the analytical arguments above, we have efficient (nonconforming) numerical strategies [31, 35, 32, 74] to discretize the minimization problem by first minimizing the extension of $\mathcal{E}_\alpha$ to $H^1(\omega,\mathbb{R}^n)$, i.e., $\tilde{\mathcal{E}}_\alpha : H^1(\omega,\mathbb{R}^n) \to \mathbb{R}$ for $\beta = 0$, vanishing magnetic potential $u$, and zero external magnetic field (i.e., here and in the following $\tilde{\mathcal{E}}_\alpha(m) = \alpha \int_\omega |\nabla m|^2 \,\mathrm{d}x$), and afterwards using stereographic projection (see Figure 2.4(c)).

Algorithm 2.1.

1. *Let $m^0 \in \mathcal{A} \cap H^1(\omega,\mathbb{R}^n)$ be an initial guess.*
2. *For every $j \ge 1$, find $\tilde{m}^j \in H^1(\omega,\mathbb{R}^n)$ such that $\tilde{\mathcal{E}}_\alpha(\tilde{m}^j) \le \tilde{\mathcal{E}}_\alpha(m^{j-1})$.*
3. *Set $m^j = \frac{\tilde{m}^j}{|\,\tilde{m}^j\,|}$.*
4. *Set $j := j+1$ and go to step 2 until a stopping criterion is met.*

A conforming finite-element realization of this algorithm confines the projection step to vertices of a quasi-uniform mesh $\mathcal{T}_h$ and computes sequences $\{m_h^j\}_j \subset \mathcal{A}_h$ from piecewise affine, globally continuous $\{\tilde{m}_h^j\}_j \subset V_h(\omega;\mathbb{R}^n)$, where

$$m_h^j \in \mathcal{A}_h \equiv \Big\{ \phi_h \in V_h(\omega;\mathbb{R}^n) \Big|\ |\,\phi_h(x_i)\,| = 1 \ \forall \text{ vertices } x_i \Big\}.$$

However, mainly because of the lack of convexity of the constraint, convergence of these algorithms cannot always be verified. In particular, the decrease in energy of this strategy can be shown if iterates $v \in H^1(\omega,\mathbb{R}^n)$ lie outside the unit ball, i.e., $|\,v(x)\,| \ge 1$, which then implies $|\,\nabla(\frac{v(x)}{|\,v(x)\,|})\,|^2 \le |\,\nabla v(x)\,|^2$, for almost every $x \in \omega$. In 1997 Alouges [2] came up with an energy-decreasing algorithm for minimizing harmonic maps, where every iteration step starts with a minimization on a new composed space, followed by a stereographic projection step: if compared to previous numerical strategies from above, this projection step now updates defects minimized on the manifold tangent to the constraint—rather than new iterates; cf. Figure 2.4(b). Once again, let $\tilde{\mathcal{E}}_\alpha$ stand only for the exchange energy term.

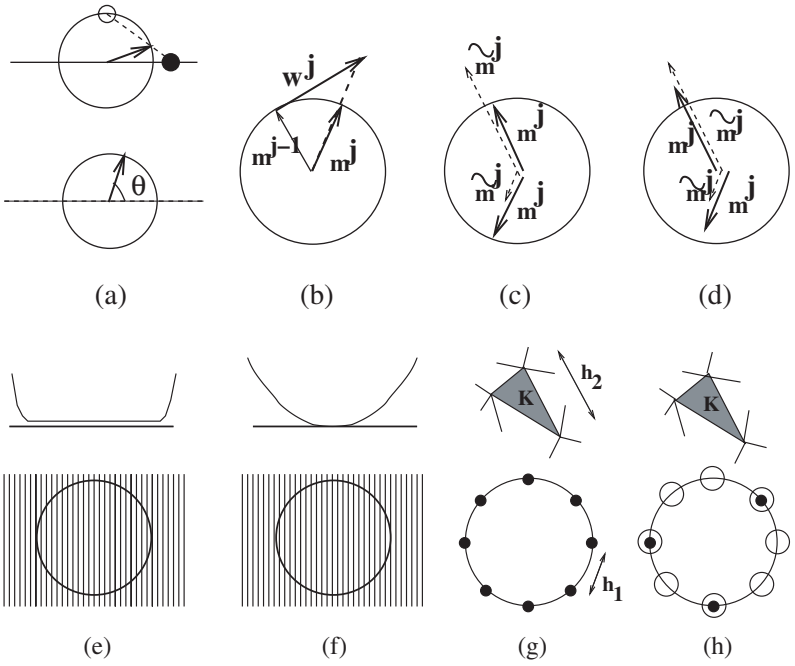


**Fig. 2.4** *Discretization of nonconvex constraint:* (a) *local charts and parameterization,* (b) *convergent discretization by Alouges,* (c) *projection onto sphere,* (d) *scaled projection,* (e) *convexified problem,* (f) *including regularization,* (g) *discrete Young-measures,* (h) *including active-set strategy.*

ALGORITHM 2.2.

1. *Let* $m^0 \in \mathcal{A} \cap H^1(\omega, \mathbb{R}^n)$ *be an initial guess.*
2. *For every* $j \geq 1$, *compute a minimizer* $w^j \in K_{m^{j-1}}$ *of*

$$\tilde{\mathcal{E}}_\alpha(m^{j-1} - w) \qquad \forall\, w \in K_{m^{j-1}} \equiv \left\{ w \in H^1_0(\omega, \mathbb{R}^n) \middle| \ \langle w, m^{j-1} \rangle_{\mathbb{R}^3} = 0 \quad \text{a.e. in } \omega \right\}.$$

3. *Set* $m^j = \frac{m^{j-1} - w^j}{|\, m^{j-1} - w^j \,|}$.
4. *Set* $j := j + 1$ *and go to step* 2 *until a stopping criterion is met.*

A stopping criterion can be that the difference of two subsequent values of $\tilde{\mathcal{E}}_\alpha$, $\tilde{\mathcal{E}}_\alpha(m^{j-1}) - \tilde{\mathcal{E}}_\alpha(m^j)$, is sufficiently small. By construction of the numerical scheme, we have

$$|\, m^{j-1} - w \,|^2 = 1 + |\, w \,|^2 \geq 1 \quad \text{a.e. in } \omega\,,$$

which implies the energy estimate $\tilde{\mathcal{E}}_\alpha(m^j) \leq \tilde{\mathcal{E}}_\alpha(m^{j-1} - w^{j-1}) \leq \tilde{\mathcal{E}}_\alpha(m^{j-1})$ during the projection step; from a practical viewpoint, the lack of convexity has been transformed into the linear, easier-to-handle constraint $\langle m^j, w \rangle_{\mathbb{R}^3} = 0$ a.e. in $\omega$. The following result is due to Alouges [2].

THEOREM 2.1. *Algorithm* 2.2 *converges in the sense that a (not relabeled) subsequence* $\{m^j\}_j$ *weakly converges in* $H^1(\omega, \mathbb{R}^3)$ *to a harmonic map* $m^\infty \in \mathcal{A} \cap H^1_{n_0}(\omega, \mathbb{R}^3)$, *where* $n_0$ *is a boundary datum of* $m^0$. *Moreover, the entire sequence* $\{w^j\}$ *strongly converges to zero in* $H^1_0(\omega, \mathbb{R}^3)$.

In [8] stability and convergence of a finite-element realization of Alouges's algorithm for restricted triangulations with angles not exceeding $\pi/2$ is verified, and

explicit counterexamples are presented (in two and three dimensions) that show an increase of energy for nonpermitted triangulations. These results apply to harmonic maps, whereas Landau–Lifshitz energy also accounts for nonlocal effects in terms of stray field energy; recently in [3] Alouges's scheme was extended to the micromagnetic energy $\mathcal{E}_\alpha$ by accounting for nonlocal stray field energies in particular. The splitting-type algorithm extends the layout of Algorithm 2.2 by introducing an additional parameter $\lambda > 0$.

ALGORITHM 2.3.

1. *Let $m^0 \in \mathcal{A} \cap H^1(\omega, \mathbb{R}^n)$ be an initial guess.*
2. *For every $j \geq 1$, compute a minimizer $w^j \in K_{m^{j-1}}$ of*

$$\alpha \int_\omega |\nabla(m^{j-1} - w)|^2 \,\mathrm{d}x + \int_\omega \varphi(m^{j-1} - w)\,\mathrm{d}x + \frac{1}{2}\int_\omega \langle \nabla\Delta^{-1}\mathrm{div}\, m^{j-1}, m^{j-1} - w\rangle_{\mathbb{R}^n}\,\mathrm{d}x - \int_\omega \langle H, m^{j-1} - w\rangle_{\mathbb{R}^n}\,\mathrm{d}x\,.$$

3. *Set $m^j = \frac{m^{j-1} - \lambda w^j}{|m^{j-1} - \lambda w^j|}$.*
4. *Set $j := j + 1$ and go to step 2 unless a stopping criterion is met.*

Different scaling properties of exchange energy and stray field energy contributions in terms of $\lambda > 0$ yield energy decay of the method during projection and hence convergence for sufficiently small choices $\lambda < \lambda_0$.

REMARK 2.1. *Alternative strategies to conserve $|m| = 1$ rest upon the parameterization of $S^{n-1}$ or local charts for the sphere (cf. Figure* 2.4(a)*), which may lead to efficient numerical methods.*

**2.3. The Relaxed Landau–Lifshitz Energy without Exchange Energy: A Mesoscopic Model.** Microscopic magnetization patterns described as minima of (1.4) reveal multiple scales, with the smallest oscillations exhibiting a scale $\alpha > 0$, allowing for infinitely many oscillations for minimizers $m \in L^\infty(\omega, \mathbb{R}^n)$ in the limiting case $\alpha = 0$. Section 2.3.1 considers mesh-dependent discrete minimizers of $\mathcal{E}_0 : \mathcal{A}_h \to \mathbb{R}$ of multiple scales to illustrate possible smearing of physical patterns (for $\alpha > 0$) due to discretization effects; this section bridges over to the study of the degenerate elliptic problem (2.5)–(2.7). Existing results on the relaxation (2.2) using Young measures are reviewed in section 2.3.3.

**2.3.1. Discretization of the Nonconvex Problem.** We highlight numerical effects imposed on $m_h = \mathrm{argmin}_\phi \mathcal{E}_0(\phi) \in \mathcal{A}_h$ by the underlying mesh $\mathcal{T}_h$ to allow for reliable resolution of relevant structures of $m = \mathrm{argmin}_\phi \mathcal{E}_\alpha(\phi) \in \mathcal{A} \cap H^1(\omega, \mathbb{R}^n)$, $\alpha > 0$ small. In [93] magnetization patterns are constructed for minimizers $m_h = \mathrm{argmin}_\phi \tilde{\mathcal{E}}_0(\phi) \in \tilde{\mathcal{A}}_h \equiv \{\phi_h|_K \in \mathcal{P}_0(K; \mathbb{R}^n)\ \forall K \in \mathcal{T}_h\}$ for uniaxial materials in the absence of an exterior magnetic field, i.e.,

$$\tilde{\mathcal{E}}_0(\phi_h) = \beta \int_\omega |\langle \phi_h, e_\perp\rangle_{\mathbb{R}^n}|^2 \,\mathrm{d}x + \frac{1}{2}\int_{\mathbb{R}^n} |\nabla\Delta^{-1}\mathrm{div}(\chi_\omega \phi_h)|^2 \,\mathrm{d}x\,. \tag{2.10}$$

Above and in the following $\mathcal{P}_d(K)$, $d = 0, 1$, denotes spaces of polynomials of degree $\leq d$ on $K$. Minimizing constructions motivate a geometry which bridges laminate structures of scale $\mathcal{O}(h^{1/3})$ in the bulk of the specimen to closure domain structures of scale $\mathcal{O}(h^{2/3})$ at the boundary $\partial\omega$ over a length scale $\mathcal{O}(1)$ in order to optimally balance interpolation errors on a quasi-uniform mesh; cf. Figure 2.5. Computing energy contributions in (2.10) which arise from interpolating this structure onto the

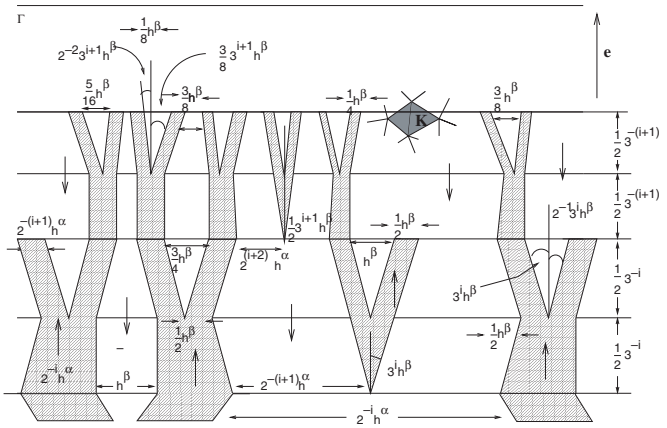


**Fig. 2.5** *Construction of branching magnetization $m_h$, using direct minimization (uniaxial; from* [93]*).*

mesh gives the upper bound for uniaxial materials [93]:

$$\min_{\phi_h \in \tilde{\mathcal{A}}_h} \tilde{\mathcal{E}}_0(\phi_h) \le C \left(1 + \log_3 \frac{1}{h}\right) h^{2/3}.$$

Interestingly, scales differ for discrete minimizing magnetizations of cubic ferromagnets, where laminates in the interior of the ferromagnet of magnitude $\mathcal{O}(1)$ are reduced to closure domains $\mathcal{O}(h)$ by multiple branching over a length scale of $\mathcal{O}(1)$; cf. [93].

**2.3.2. Discretization of the Convexified Problem.** Computations of the mesoscopic magnetization are more efficient if (2.5)–(2.7) are used, rather than dealing with the minimization problem $\tilde{\mathcal{E}}_0 : \tilde{\mathcal{A}} \to \mathbb{R}$ directly, in cases where the convex envelope $\varphi^{**} : \mathbb{R}^n \to \mathbb{R} \cup \{+\infty\}$ is explicitly known. This is the case of uniaxial materials where $\varphi^{**}(m)$ is quadratic in all components of $m$ perpendicular to $e$, provided $|m| \le 1$. These equations are degenerate elliptic, so solutions $(m, u, \lambda) \in L^2(\omega, \mathbb{R}^n) \times H^1(\mathbb{R}^n) \times L^2(\omega)$ are not unique in general. However, they are unique for uniaxial materials in two or three dimensions (cf. [21] for the first proof in two dimensions). We recall the proof from [67]. Note that the difference of two possible solutions $(\delta, \tilde{e}) := ((m_2 - m_1)\chi_\omega, u_2 - u_1)$ to (2.5)–(2.7) is determined by

(2.11)
$$\| \nabla \tilde{e} \|^2_{L^2(\mathbb{R}^n)} + \int_\omega \left\langle D\varphi^{**}(m_2) - D\varphi^{**}(m_1), \delta \right\rangle_{\mathbb{R}^n} \mathrm{d}x + \int_\omega \left\langle \lambda_2 m_2 - \lambda_1 m_1, \delta \right\rangle_{\mathbb{R}^n} \mathrm{d}x = 0.$$

By monotonicity arguments, it is easy to see that all terms are nonnegative and hence vanish, yielding

$$e = 0, \qquad \operatorname{div} \delta = 0 \quad \text{a.e. in } \omega, \qquad \langle \delta, n \rangle_{\mathbb{R}^n} = 0 \quad \text{a.e. on } \partial\omega,$$

where for a moment $n$ denotes the outer unit normal to $\partial\omega$. Here, the last two results are outcomes of the first one, using (1.1). As $\varphi^{**}$ is strictly convex in all components perpendicular to $e$, then $\delta$ can have only one nonzero component (the one parallel to $e$). At the same time, $\operatorname{div} \delta = 0$ and therefore it depends only on $n - 1$ variables. Since $\delta$ has compact support it must vanish identically. These arguments do not carry over to cubic materials.

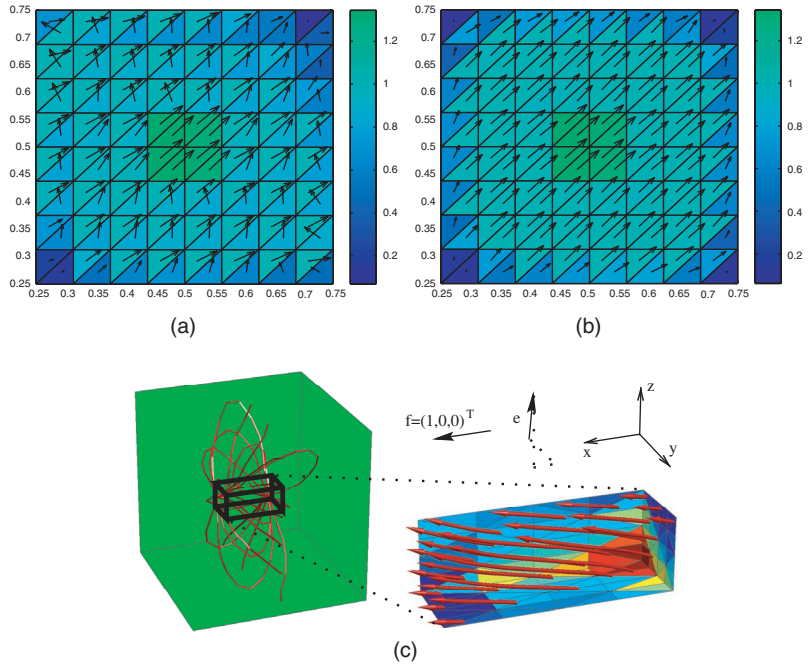


**Fig. 2.6** *Convexification: magnetization of* (a) *unstable scheme,* (b) *stable scheme (Problem* 2.1*),* (c) *stabilized scheme (Problem* 2.2*,* $\ell = A$*) (from* [93, 47]*).*

A canonical conforming finite-element discretization of (2.5)–(2.7) asks for solutions $(m_h, u_h) \in W_h(\omega;\mathbb{R}^n) \times V_h(\mathbb{R}^n)$, where $V_h(\cdot)$ is assembled from elementwise affine, globally continuous functions, and $W_h(\cdot)$ gathers elementwise constant grid functions on a quasi-uniform mesh $\mathcal{T}_h$ of $\mathbb{R}^n$ such that $\mathcal{T}_h\big|_\omega$ is a triangulation of $\omega \subset \mathbb{R}^n$; the nonstable behavior is illustrated by the computations in Figure 2.6(a). Mathematically, this observation may be explained by the lack of validity of the discrete Helmholtz principle for the use of a finite-element pairing, which was the crucial tool to verify the uniqueness of solutions for the limiting problem (2.5)–(2.7) in the above argument. This shortcoming of the discretization is cured if $V_h(\cdot)$ is replaced by Crouzeix–Raviart-based elements

$$\tilde{V}_h(\Omega) = \left\{ \phi_h \in L^2(\Omega) \big|\ \phi_h\big|_K \in \mathcal{P}_1(K),\ \int_{\overline{K}\cap\overline{K'}} \phi_h \,\mathrm{d}s = 0 \quad \forall K, K' \in \mathcal{T}_h \right\}$$

for polyhedral $\Omega \subseteq \mathbb{R}^n$, which now allows for the discrete Helmholtz principle of involved spaces, leading to a well-posed discretization [21] of (2.5)–(2.7) (uniaxial materials). In [21] a penalized version of this problem is then studied, and nonlocal magnetostatic effects are accounted for on a set $\mathbb{R}^n \supseteq \Omega \supset \omega$ using vanishing Dirichlet data for the magnetic potential, i.e., $u_h \in \tilde{V}_h^0(\Omega)$; see also Figure 2.4(e).

PROBLEM 2.1. *Find* $(m_h, u_h) \in W_h(\omega;\mathbb{R}^n) \times \tilde{V}_h^0(\Omega)$ *such that*

$$(\nabla_h u_h, \nabla_h w_h) = (m_h, \nabla_h w_h) \quad \forall\, w_h \in \tilde{V}_h^0(\Omega)\,,$$

$$\nabla_h u_h + D\varphi^{**}(m_h) + \lambda_h m_h = P_h H, \qquad \lambda_h = \varepsilon^{-1}\frac{(|\,m_h\,|-1)_+}{|\,m_h\,|} \quad \text{a.e. in } \omega\,.$$

A proof of the following error statement for solutions to Problem 2.1 (uniaxial case) exploits the discrete Helmholtz principle for the finite pairing used and a bootstrapping argument [21]:

(2.12)
$$\|\nabla(u-u_h)\|^2_{L^2(\Omega)}+\| D\varphi^{**}(m)-D\varphi^{**}(m_h)\|^2_{L^2(\omega,\mathbb{R}^2)}+\|\lambda m-\lambda_h m_h\|^2_{L^2(\omega,\mathbb{R}^2)} \le C\big(\varepsilon+h\big)\,.$$

An alternative way to obtain a stable discretization of (2.5)–(2.7) is to go back to the formerly mentioned scenario $(m_h,u_h)\in W_h(\omega;\mathbb{R}^n)\times V_h^0(\Omega)$ and add stabilizing terms which control nonphysical oscillatory behavior.

PROBLEM 2.2. *Find* $(m_h,u_h)\in W_h(\omega;\mathbb{R}^n)\times V_h^0(\Omega)$ *such that, for* $\ell\in\{A,B\}$,

$$(\nabla u_h,\nabla w_h)=(m_h,\nabla w_h)\quad\forall\, w_h\in\tilde V_h^0(\Omega)\,,$$
$$(\nabla u_h,\mu_h)+(D\varphi^{**}(m_h),\mu_h)+(\lambda_h m_h,\mu_h)+t_\ell([m_h],[\mu_h])=(H,\mu_h)\quad\forall\,\mu_h\in W_h(\omega,\mathbb{R}^n)\,,$$
$$\lambda_h=\varepsilon^{-1}\frac{(|\,m_h\,|-1)_+}{|\,m_h\,|}\qquad a.e.\ in\ \omega\,.$$

Here, $[\cdot]$ denotes the jump across interelement interior faces $\xi\equiv\overline{K}\cap\overline{K'}\in\Xi$ for adjacent $K,K'\in\mathcal{T}_h\big|_\omega$. The following stabilizations are considered in [93, 47] for $n=2$:

$$t_A\big([m_h],[\mu_h]\big)=\sum_{\xi\in\Xi}h_\xi\int_\xi[\langle m_h,n\rangle_{\mathbb{R}^2}][\langle\mu_h,n\rangle_{\mathbb{R}^2}]\,\mathrm{d}x\,,$$
$$t_B\big([m_h],[\mu_h]\big)=\sum_{\xi\in\Xi}h_\xi\int_\xi\langle[m_h],[\mu_h]\rangle_{\mathbb{R}^2}\,\mathrm{d}x\,.$$

Problem 2.2 produces solutions which satisfy (2.12) for slightly restricted mesh geometries; its convergence proof avoids the above argument based on the discrete Helmholtz principle and uses inverse-type inequalities instead. The behavior of this stabilized method can be motivated by interpreting Problem 2.2 as a Kuhn–Tucker equation of a slight modification of the strictly convex energy ($\varepsilon>0$)

$$\tilde{\mathcal{E}}_0(m)+\varepsilon\int_\omega\mathfrak{Z}_\ell(m)\,\mathrm{d}x\,,\qquad\mathfrak{Z}_A(m)=|\,\mathrm{div}\,m\,|^2\quad\text{or}\quad\mathfrak{Z}_B(m)=|\,\nabla m\,|^2\,.$$

Convergence result (2.12) allows for control of certain components of iterates $\{m_h\}_h$ as $h\to0$, obtained from Problems 2.1 and 2.2; in general, strong convergence of $\{m_h\}_h$ may not be expected due to the degenerate convexity of the energy functional (2.4), which prevents us from reliably recovering the uniquely defined Young measure in the uniaxial case (cf. [36] and section 2.3.3)

$$x\mapsto\nu_x=\Gamma(m(x))\delta_{m^+(m(x))}+\Big(1-\Gamma(m(x))\Big)\delta_{m^-(m(x))}\,,\quad\text{where}\tag{2.13}$$
$$m^\pm\big(m(x)\big)=\pm\Big(1-\langle m(x),e_\perp\rangle^2_{\mathbb{R}^2}\Big)^{1/2}e+\langle m(x),e_\perp\rangle_{\mathbb{R}^2}e_\perp\,,$$
$$\Gamma\big(m(x)\big)=\frac12+\frac{\langle m(x),e\rangle_{\mathbb{R}^n}}{2\big(1-\langle m(x),e_\perp\rangle^2_{\mathbb{R}^2}\big)^{1/2}},$$

in a postprocessing step. Surprisingly, numerical schemes can be constructed for the uniaxial case which compute magnetizations that strongly converge to solutions of (2.5)–(2.7) and which are motivated by

$$\tilde{\mathcal{E}}_0(m)+\varepsilon_1\int_\omega|\,\nabla m\,|^2\,\mathrm{d}x+\varepsilon_2\int_\omega|\,\nabla^2 m\,|^2\,\mathrm{d}x\,,\qquad\varepsilon_i>0\,.\tag{2.14}$$

The following scheme uses piecewise affine finite elements for the magnetization field as well [93]; cf. Figure 2.4(f).

PROBLEM 2.3. *Find* $(m_h, u_h) \in V_h(\omega, \mathbb{R}^2) \times V_h^0(\Omega)$ *such that*

$$
\begin{aligned}
&(\nabla u_h, \nabla w_h) = (m_h, \nabla w_h) \quad \forall\, w_h \in V_h^0(\Omega)\,,\\
&(\nabla u_h, \mu_h) + (\langle m_h, e_\perp\rangle_{\mathbb{R}^2}, \langle \mu_h, e_\perp\rangle_{\mathbb{R}^2}) + (\lambda_h m_h, \mu_h)\\
&\qquad + h \sum_{\xi\in\Xi} \int_\xi \langle [\partial_n m_h], [\partial_n \mu_h]\rangle_{\mathbb{R}^4} + h^{3/2}(\nabla m_h, \nabla \mu_h) = (H, \mu_h) \quad \forall\, \mu_h \in V_h(\omega, \mathbb{R}^2)\,,\\
&\lambda_h = h^{-2}\frac{(|\, m_h\,| - 1)_+}{|\, m_h\,|} \qquad \text{a.e. in } \omega\,.
\end{aligned}
$$

Note the scaling for $\lambda_h$, which is different from the one in Problems 2.1 and 2.2. Next to (2.12), the results

$$
\begin{aligned}
(2.15)\qquad &\frac{\sqrt{h}}{2}\left(\sum_{\xi\in\Xi}\int_\xi |\,[m - m_h]\,|^2\,\mathrm{d}x\right)^{1/2} + h^{1/2}\|\, m - m_h\,\|_{L^2(\omega,\mathbb{R}^2)}\\
&\qquad + h^{3/4}\|\,\nabla(m - m_h)\,\|_{L^2(\omega,\mathbb{R}^4)} \le C\,h\,,\\
(2.16)\qquad &\|\, m - m_h\,\|_{L^2(\omega',\mathbb{R}^2)} \le C\Big(h^{5/8} + \mathrm{dist}^{-1/2}(\partial\omega, \omega')h^{3/4}\Big)
\end{aligned}
$$

apply [93], provided that the solution to (2.5)–(2.7) is sufficiently regular; the proof is based on a Helmholtz decomposition for $L^2(\omega, \mathbb{R}^2)$ functions, making use of the increased stability properties of the scheme, together with estimates for $\|\, m - m_h\,\|_{H^{-1}(\omega,\mathbb{R}^2)}$; finally, balancing the error in the interior of $\omega \subset \mathbb{R}^2$ and in a boundary layer close to $\partial\omega$ yields (2.15)–(2.16). Control of the related Young measure is now an immediate consequence.

REMARK 2.2. *Computation of the nonlocal magnetostatic field* $-\nabla u$ *requires solving* (2.5) *in the whole* $\mathbb{R}^n$. *There are different approaches to evaluating this field. First, truncate by restricting the magnetostatic field to the compact domain* $\Omega$ *for* $\mathbb{R}^n \supset \Omega \ni \omega$ *and impose Dirichlet data on* $\partial\Omega$*; see, e.g.,* [21, 93]. *Choosing* $\operatorname{diam}\Omega \approx 10\operatorname{diam}\omega$ *is motivated in* [44] *for practical studies in order to capture relevant magnetostatic energy contributions. Second,* (2.5) *is solved exactly in* [76, 75, 69, 91, 20] *via integral representation, i.e.,* $-\nabla u = -\nabla\mathcal{L}m$, *for a linear convolution operator* $\mathcal{L} : L^2(\mathbb{R}^n, \mathbb{R}^n) \to H^1(\Omega)$*; interesting numerical approaches using* $\mathcal{H}$*-matrix techniques in this context are proposed and studied in* [91]. *We refer to Figure* 2.7 *for a comparison of these strategies for computing the stray field.*

**2.3.3. Discretization of the Relaxed Problem.** If the convex envelope $\varphi^{**}$ is not known explicitly, minimizing $\overline{\mathcal{E}}_0$ from (2.2) yields a measure-valued solution which contains information not only about the mesoscopic magnetization $m$ but also about a pattern of minimizing sequences. As to a numerical discretization of (2.2), we might also need, besides a discretization of $\omega$, a discretization of the sphere $S^{n-1}$; cf. Figure 2.4(g). Let $\mathcal{T}_{h_1}^1$ be a quasi-uniform triangulation of $\omega$ that consists of elements with diameter not exceeding $h_1$. Similarly, we define a triangulation $\mathcal{T}_{h_2}^2$ of $S^{n-1}$ which is assembled from elements with a spherical diameter not exceeding $h_2$. Hence, we obtain a triangulation $\mathcal{T}_h = \mathcal{T}_{h_1}^1 \times \mathcal{T}_{h_2}^2$ of $\omega \times S^{n-1}$ with mesh parameter $h = (h_1, h_2)$. We may now define projectors $P_{h_1}^1 : L^1\big(\omega; C(\mathcal{S}^{n-1})\big) \to L^1\big(\omega; C(\mathcal{S}^{n-1})\big)$ by

$$
[P_{h_1}^1 G](x, A) = \frac{1}{|K|}\int_K G(y, A)\,\mathrm{d}y \qquad \forall\, x \in K \in \mathcal{T}_{h_1}^1\,,
$$

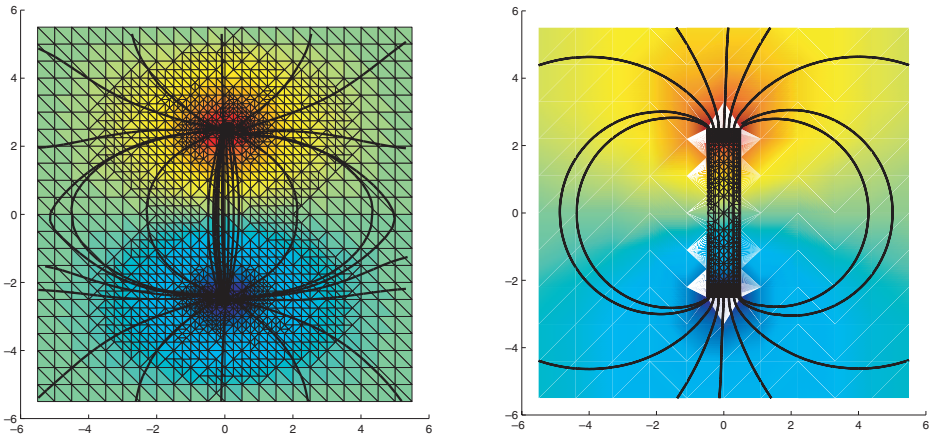

**Fig. 2.7** *Stray field $-\nabla u_h$ around ferromagnet $\omega = (-0.5, 0.5) \times (-2.5, 2.5)$ displayed by level lines using truncated domain $\Omega = (-5.5, 5.5)^2$ (left) or FEM-BEM coupling (right) (from* [19]*).*

and $P^2_{h_2}(x,\cdot)$ denotes a projector that assigns to each $G(x,\cdot)$ its $\mathcal{T}^2_{h_2}$-elementwise affine, globally continuous interpolation, i.e., $[P^2_{h_2}G](x,A) = \sum_{i=1}^{L_{h_2}} G(x,A_i)v_i(A)$, for basis functions $\{v_i\}_i$ satisfying $v_i(A_j) = \delta_{ij}$; functions $v_i$ are nonnegative and $\sum_{i=1}^{L_{h_2}} v_i(A) = 1$. Then the composed projector $P_h = P_{(h_1,h_2)} = P^1_{h_1}P^2_{h_2} = P^2_{h_2}P^1_{h_1}$ provides an $\omega$-elementwise constant and $\mathcal{S}^{n-1}$-elementwise affine, globally continuous approximation, with adjoint projector $P^*_h : \overline{\mathcal{A}} \to \overline{\mathcal{A}}$ defined by $\langle \nu, P_h G\rangle = \langle P^*_h \nu, G\rangle$. The following characterization of $\overline{\mathcal{A}}_h = P^*_h \overline{\mathcal{A}} \subset \overline{\mathcal{A}}$ is taken from [94, sect. 3.5]:

$$\overline{\mathcal{A}}_h := \left\{ \nu^h = \{\nu^h_K\}_{K\in\mathcal{T}^1_{h_1}},\ \nu^h_K = \sum_{i=1}^{L_{h_2}} \lambda_{K,i}\delta_{A_i} \quad \forall\, K \in \mathcal{T}^1_{h_1} \right\},$$

where $\lambda_i\big|_K \equiv \lambda_{K,i}$ is $\mathcal{T}^1_{h_1}$-elementwise constant such that $\sum_{i\geq 1}\lambda_i = 1$. A proper discretization of (2.2) can now be stated in the following form [69]; see Figure 2.4(g).

PROBLEM 2.4. *Find a minimizer $(\mu^h) \in \overline{\mathcal{A}}_h$ of $\overline{\mathcal{E}}_0$ subject to*

$$m_{h_1}\big|_{K\in\mathcal{T}^1_{h_1}} = \int_{S^{n-1}} A\mu^h_K(\mathrm{d}A),\ (\nabla_{h_1}u_{h_1}, \nabla_{h_1}w_{h_1}) = (m_{h_1}, \nabla_{h_1}w_{h_1})\,\forall\, w_{h_1} \in \tilde{V}^0_{h_1}(\Omega)\,.$$

Problem 2.4 is convex, of quadratic-linear type, and with linear constraint; a numerical analysis is given in [69], which verifies convergence of the method for a relative scaling $h_2 = o(h_1^{n/2})$. In practice the size of this problem may be very large for sufficiently small $h$. In [69], and motivated by [22], an active-set strategy is proposed and analyzed which selects active atoms for each element $K \in \mathcal{T}_{h_1}$ independently according to a local convex optimization problem; see Figure 2.4(h). This procedure drastically decreases the complexity of the problem; we refer to [69] for details.

REMARK 2.3. *Let us mention another possibility for approximating the relaxed problem by means of Young measures. Using the Carathéodory theorem, we know that for any $m(x) \in \mathbb{R}^n$, $|m(x)| \leq 1$, there are at most $n+1$ points $A_i$ on $S^{n-1}$ such that $\varphi^{**}(m) = \sum_{i=1}^{n+1}\lambda_i\delta_{A_i}$, where functions $\lambda_i$, $i = 1,\dots,n+1$, are coefficients of a convex combination. Therefore, we can consider a Young measure $\nu^h_K = \sum_{i=1}^{n+1}\lambda_{K,i}\delta_{A_i}$, where $K \in \mathcal{T}^1_{h_1}$ and $\{\lambda_{K,i}\}_i$ are constant on $K$. Points $\{A_i\}_i \in S^{n-1}$ may again be described*

*by means of angles in spherical coordinates to avoid the nonconvex constraint, and for each* $K \in \mathcal{T}_{h_1}^1$ *we hold* $\{\lambda_{K,i}\} \geq 0$ *and* $\sum_{i=1}^{n+1} \lambda_{K,i} = 1$. *However, the resulting optimization problem is highly nonconvex; see* [66] *for details.*

**2.4. Thin Film Limit.** Driven by the needs of spin electronics, ferromagnetic films enjoy renewed attention. The magnetization patterns are different from those in bulk materials because the magnetostatic interaction behaves differently if the magnetization $m : \omega \to \mathbb{R}^3$ remains uniform across the thickness of the film. Let $\omega = \omega' \times (0, \delta)$ be a cylindrical domain of radius $\ell$ and thickness $\delta > 0$, $\delta \ll \ell$, and $\varphi(m) = \beta\,(m_2^2 + m_3^2)$ for $m = (m_1, m_2, m_3)$, i.e., the easy axis is in the plane of the film. Under the assumptions that (i) the sample is not too small in the sense of $\alpha \ll \ell\delta \log^{-1}\left(\frac{\ell}{\delta}\right)$, and (ii) anisotropy and the external field are sufficiently weak in the sense of $\beta = \mathcal{O}(\frac{\delta}{\ell})$ and $|\,H\,| = \mathcal{O}(\frac{\delta}{\ell})$, it is shown in [38] that the limiting behavior of minimizers of (1.4) for $\delta \to 0$ may be represented by the following two-dimensional reduced problem: Minimize

$$\tilde{\mathcal{E}}_{\text{thin}}(m') = \frac{\beta}{\delta} \int_{\omega'} |\,m_2'\,|^2 \,\mathrm{d}x' + \frac{1}{2} \int_{\Omega} |\,\nabla \tilde{u}\,|^2 \,\mathrm{d}x - \frac{1}{\delta} \int_{\omega'} \langle H, m' \rangle_{\mathbb{R}^n} \,\mathrm{d}x' \tag{2.18}$$

among all $m' : \omega' \to \mathbb{R}^2$, $\tilde{u} : \Omega \to \mathbb{R}$, for $\Omega \subseteq \mathbb{R}^3$ containing $\omega$, such that

$$|\,m'\,|^2 \leq 1 \quad \text{in } \omega', \qquad (\nabla \tilde{u}, \nabla w) = (m', \nabla' w') \quad \forall\, w \in H_0^1(\Omega)\,.$$

This result can be motivated by a simple scaling argument, according to which the surface, the anisotropy, and Zeeman's energy, respectively, are of magnitudes $\mathcal{O}(\alpha\delta)$, $\mathcal{O}(\beta\ell^2\delta)$, and $\mathcal{O}(|\,H\,|\ell^2\delta)$. The magnetostatic energy, being nonlocal, is more complicated but can be approximated by [44, 38]

$$\int_{\Omega} |\,\nabla u\,|^2 \,\mathrm{d}x \approx \delta^2 \int_{\Omega} |\,\nabla \tilde{u}\,|^2 \,\mathrm{d}x + \delta \int_{\omega'} |\,m_3\,|^2 \,\mathrm{d}x' = \mathcal{O}(\ell\delta^2) + \mathcal{O}(\ell^2\delta)\,.$$

This formula splits magnetostatic contributions into those which penalize the in-plane divergence and the out-of-plane component separately.

In the regime $\delta \ll \ell$ the larger of the two magnetostatic terms is the cost of the out-of-plane component $m_3$, which is why we expect $m_3 \approx 0$. Assuming now $m(x) = m(x')$ for $x' \in \mathbb{R}^2$ and using the above scalings for $\beta, |\,H\,|$, all terms—apart from the smaller surface exchange energy—lead to contributions $\mathcal{O}(\ell\delta^2)$, which motivates (2.18). We refer to [40] for further details.

**3. Dynamical Models: From Spin Dynamics to Mesoscopic Evolution.** Field-induced magnetization dynamics in a ferromagnetic body leads to domain-wall motion to reach states of lower energy. During this motion, the domain wall may be trapped in local energy minima until thermal fluctuations allow it to overcome one of the energy barriers that separate the system from neighboring favorable states; a full description of magnetization reversal needs to contain precisely the spatial and time dependence of the nucleation and domain-wall structure at different fields: at low fields, and for an initially saturated sample, nucleation always initiates at low anisotropic extrinsic defects or at film edges; in contrast, at high fields, intrinsic nucleation takes place in many low-coercivity regions, e.g., correlated with film polycrystallinity in composed matter. Rough domain walls move in a jerky manner by successive micrometer-sized jumps at the wall boundary; moreover, submicron-sized defects and film nanostructure are further impedences of domain-wall propagation at lower scales.

Up to now, the most rigorous micromagnetic model has seemed to be the Landau–Lifshitz model. However, this microscopic description models phenomena that are reasonable only for small areas of submicron size and cannot model large Barkhausen jumps, for example. Moreover, relevant time scales are of picoseconds, and the relaxation of magnetization can be examined only across no more than a few nanoseconds. These shortcomings are among the main motivations for mesoscopic models to describe magnetization reversal.

**3.1. The Model by Landau and Lifshitz.** The foundation of magnetization precession is laid by quantum mechanics, where the mean value of the spin operator $S$ evolves according to Schrödinger's equation:

$$\frac{d}{dt}\langle S\rangle(t) = \frac{g\mu_B}{h}\langle S\rangle(t) \times B(t)\,,$$

where $B(t) = \mu_0 H(t)$. If the magnetization $m : \omega \to S^2$ is understood to be the dipole of spins per unit volume, we arrive at the Landau–Lifshitz equation, governing magnetization motion, i.e.,

$$m_t(t) = \gamma_0\, m(t) \times H(t)\,. \tag{3.1}$$

Assuming the magnetic field to be time independent, successive multiplication by $m$ and $H$ leads to

$$\frac{d}{dt}|\, m(t)\,|^2 = 0\,, \qquad \frac{d}{dt}\langle m(t), H\rangle = 0\,.$$

Hence, the modulus of the magnetization remains unchanged during motion, and the angle between the magnetization and $H$ also remains constant as a function of time. The Landau–Lifshitz model therefore describes a precessional motion of the magnetization around the applied field, as sketched in Figure 1.3, and the angular frequency is a linear function of the magnetic field, $\omega_0 = \gamma_0|\, H\,|$. The possibility of infinitely fast precession in finite time is evidenced by the following example (from [29]).

EXAMPLE 3.1. *Let $a, m_0 \in \mathbb{R}^3$. Then the unique solution of $m_t(t) = a \times m(t)$, $t > 0$, for $m(0) = m_0$ is given by the unimodular evolution*

$$m(t) = \exp(at) \times m_0 = m_0^{\parallel} + m_0^{\perp}\cos\big(|\, a\,|t\big) + \frac{a}{|\, a\,|} \times m_0^{\perp}\sin\big(|\, a\,|t\big)$$

*for $m_0 = m_0^{\perp} + m_0^{\parallel}$, where $m_0^{\parallel}$ is parallel to $a$ and $m_0^{\perp}$ is perpendicular to $a$.*

From a mathematical viewpoint, it is only recently that solution concepts have been studied for the Landau–Lifshitz equation in the form $m_t = m \times \Delta m$ for $m : \omega \to S^2$ and $\omega \subset \mathbb{R}^2$. The existence of weak solutions to the related Cauchy problem goes back to [102], and the global existence of smooth solutions for small initial energies ($n = 2$) is studied in [24, 102]; an open question is on the existence of a global smooth solution of the Landau–Lifshitz equation for $n \geq 2$. The existence of (finite-energy) finite-time singularities also plays an important role in establishing the uniqueness of solutions; in particular, when the singularities are weak enough, solutions can be extended in a weak sense beyond the singularity, possibly in a nonunique fashion. The question of whether weak solutions are unique is not known for the two-dimensional Landau–Lifshitz equation; there are different characterizations of weak solutions, and it is not clear whether they coincide. For the related equations of harmonic map

heat flow and wave maps, there exist nonunique solutions due to the appearance of singularities [33].

From a physical viewpoint, the mathematical concept of singularities translates to defects and spatial energy concentration in ferromagnetic materials. The issue of nonuniqueness is important for micromagnetic simulation. Understanding the source and characterizing the nature of singularities affect the validity of the physical model as well as what allowable features should be present in the definition of a weak solution.

Another well-known approach to studying the Landau–Lifshitz equation and its possible singularities rewrites the problem as a perturbed version of the cubic nonlinear Schrödinger equation by stereographically projecting the target sphere $S^2$ onto the complex plane, $q_t = i\Delta q + \partial^{-1}(|\, q^2\,|^2)\partial q + \mathcal{O}(q^3)$. The main motivations of this approach are

1. the equivalence of $m_t = m \times m_{xx}$ with the cubic nonlinear Schrödinger equation $q_t = i(q_{xx} + |\, q\,|^2 q)$ in one space dimension, using the Hasimoto transform; and
2. the extensive results available on the solution's behavior for the cubic nonlinear Schrödinger equation $q_t = i(\Delta q - |\, q\,|^2 q)$ in higher dimensions: for $n < 2$, no singularities appear, whereas singularities can form in the critical and supercritical cases $n \geq 2$.

The studies in 2 above benefit heavily from the underlying principles of conservation of $\|\, q\,\|_{L^2}$, i.e., multiply by $\overline{q}$ and take the real part, and energy $E(q) = \frac{1}{2}\int_\omega |\, \nabla q\,|^2\, \mathrm{d}x - \frac{1}{4}|\, q\,|^4\, \mathrm{d}x$, i.e., multiply by $\overline{q}_t$ and take the imaginary part. Unfortunately, part of the analytical methods used to study the blow-up behavior of solutions to the cubic nonlinear Schrödinger equation fails in the context of the Landau–Lifshitz equation (cf. [62]), which motivates numerical studies instead.

**3.1.1. Discretization of Landau–Lifshitz Equation.** It is due to the highly nonlinear character of $m_t = m \times \Delta m$ that explicit time integrators are often given preference over implicit ones. However, only high-order explicit discretizations possess nontrivial stability regions in this case, as detailed in [110]; the following observation is taken from this reference.

EXAMPLE 3.2. *Let $a, m_0 \in \mathbb{R}^3$. The discretization of the problem $m_t(t) = a \times m(t)$, $t > 0$, for $m(0) = m_0$ by explicit Euler reads*

$$m^{j+1} = m^j - k\, a \times m^j \equiv A m^j\,, \qquad m^0 = m_0\,.$$

*The three eigenvalues of $A$ are $\lambda_1 = 1$, $\lambda_2 = 1 + |\, a\,|ki$, and $\lambda_3 = 1 - |\, a\,|ki$; hence, $\rho(A) = \sqrt{1 + |\, a\,|^2 k^2} > 1$. This implies that the stability region for the Euler scheme contains only $\{k = 0\}$.*

This observation results from the fact that stability regions of the explicit Euler method do not contain any part of the imaginary axis except the origin. On the other hand, the stability regions of the classical third- and fourth-order Runge–Kutta schemes do contain part of the imaginary axis. For example, the absolute stability of the fourth-order explicit Runge–Kutta scheme to solve $m_t(t) = a \times m(t)$, $m(0) = m_0$, holds for cases $k = \mathcal{O}(\frac{1}{|\, a\,|})$; see [110]. This shortcoming of the explicit first-order method can be cured by artificially injected dissipative mechanisms during the computation. One possibility is a semi-implicit (Gauss–Seidel) strategy, yielding absolute stability for choices $k = \mathcal{O}(\frac{1}{|\, a\,|})$. If applied to $m_t(t) = m(t) \times \Delta m(t)$, the following semidiscretization in time is proposed in [110] to compute iterates $\{m^j\}_{1 \leq j \leq J}$ for $m^j = (m_1^j, m_2^j, m_3^j)$.

ALGORITHM 3.1.
1. *Let* $m^0 = m_0$.
2. *Given* $m^j$, $0 \le j \le J$, *find* $m^{j+1}$ *that solves*

$$\begin{pmatrix} m_1^{j+1} \\ m_2^{j+1} \\ m_3^{j+1} \end{pmatrix} = \begin{pmatrix} m_1^j + k\,(m_3^j \Delta m_2^j - m_2^j \Delta m_3^j) \\ m_2^j + k\,(m_1^{j+1} \Delta m_3^j - m_3^j \Delta m_1^{j+1}) \\ m_3^j + k\,(m_2^{j+1} \Delta m_1^{j+1} - m_1^{j+1} \Delta m_2^{j+1}) \end{pmatrix}.$$

An implicit variant of this scheme is discussed in [110] as well, and computational experiments motivate its unconditional stability.

A different strategy to obtain a convergent discretization of the Landau–Lifshitz equation was realized in [9], where the Landau–Lifshitz equation is approximated by the LLG equation (3.2) for $H_{\text{eff}} = \Delta m$; this approach uses artificial additional damping, which comes from the term headed by $\alpha_1 > 0$. For choices $k = o\big(\frac{\alpha_1^2 h^2}{(1+\alpha_1^2)^2}\big)$, convergence on quasi-uniform meshes $\mathcal{T}_h$ of Algorithm 3.3 can be verified. The following example is taken from [9].

EXAMPLE 3.3. *Let* $\omega = (-0.5, 0.5)^2$. *Choose initial data* $m_0 \in L^\infty(\omega, S^2)$ *as*

$$m_0(x,y) = \begin{cases} (0,0,-1) & \text{for } r > \frac{1}{2}, \\ \frac{1}{a^2+r^2}(2ax, 2ay, a^2 - r^2) & \text{for } r \le \frac{1}{2} \end{cases}$$

*for* $r = r(x,y) = \sqrt{x^2+y^2}$ *and* $a = a(x,y) = (1-2r)^4$. *Figure* 3.1 *evidences finite-time blow-up, followed by the instantaneous switching of magnetization at the origin from* $(0,0,-1)$ *to* $(0,0,1)$*; cf. also Figure* 1.3(a). *Note that the energy identity* $\frac{d}{dt} I(m,t) = 0$ *is valid throughout the experiment, where* $I(m,t) = \frac{\alpha_1}{1+\alpha_1^2} \int_0^t \| m_t(s) \|^2 \, \mathrm{d}s + \frac{1}{2} \| \nabla m(t) \|^2$ *for* $\alpha_1 = 1, \frac{1}{4}, \frac{1}{16}$.

Hysteresis curves usually tell us that beyond some value of the applied field, any magnetic sample can be considered saturated. The magnetization is then uniform and aligned with the field. Precession alone does not allow us to reach that limit, contradicting experimental evidence. Therefore, the precession equation has to include a damping term so that, after some finite time, the magnetization becomes aligned with the applied field. By far, the simplest way of introducing a damping term to (3.1) consists in replacing the field $H$ by an effective field including an ohmic-type dissipation term, $H_{\text{eff}} = H - \frac{\alpha}{\gamma_0 M_s} m_t$, where $M_s$ is the saturation magnetization and $\alpha > 0$ is a phenomenological damping parameter. One also often refers to Rayleigh-type dissipation because the associated dissipation function is a combination of the generalized velocities squared. We then obtain the LLG equation

$$m_t(t) = \gamma_0\, m(t) \times H(t) - \frac{\alpha}{M_s}\, m(t) \times m_t(t)\,.$$

The effect of damping is illustrated in Figure 1.3(b): as time passes, the magnetization spirals down until it becomes aligned with the field, and all torques acting on $m$ then vanish. The study of the LLG equation is the subject of the next section.

**3.2. The Model by Landau, Lifshitz, and Gilbert.** When the effective magnetic field $H_{\text{eff}}$ varies in time, the configuration $(m,u)$ may eventually start to evolve too. Depending on the considered scales, different models are used to describe highly nonlinear phenomena: at a microscopic level, the LLG model is used to describe the evolution of domains and structured domain walls (Bloch walls, Néel walls, cross-tie

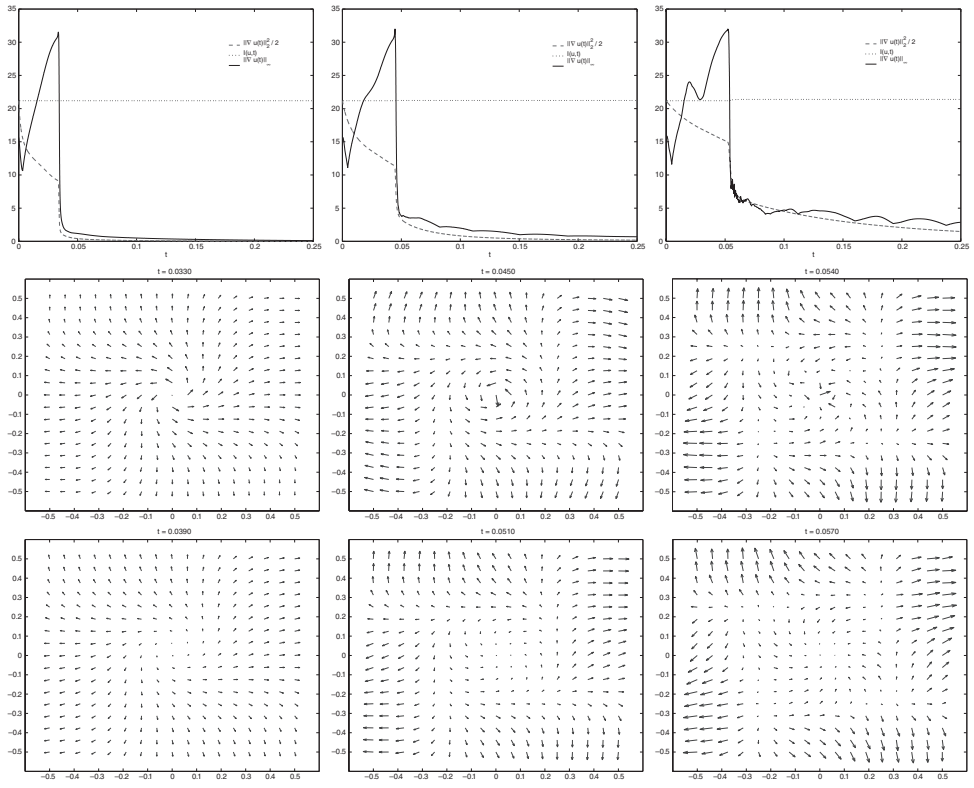


**Fig. 3.1** *Computational evidence for finite-time blow-up and switching at* $(0,0)$*: corresponding plots for* $\frac{1}{2}\|\nabla m\|_2^2$ *vs.* $\|\nabla m\|_\infty$ *(first row), and magnetization patterns close to (second row) and after (third row) blow-up time, for different damping parameters* $\alpha_1 = 1, \frac{1}{4}, \frac{1}{16}$ *(columnwise) (from* [9]*).*

walls, etc.) or codimension-2 defects called vortices in thin films; although small in dimension, they enforce a nontrivial topological arrangement of the magnetization field. Spin dynamics ("magnetization reversal") from millisecond down to femtosecond time scales in magnetic materials of micrometers down to dozens of nanometers is the key for fast data storage in hard disks. One certain disadvantage of the model is that it describes the evolution of pronounced microstructures rather than averaged magnetic properties; hence, phenomenological rate-independent models motivated from those in plasticity theory are used to describe magnetization dynamics on a mesoscopic level, as will be further detailed in section 3.3.

The LLG equation [73] describes the evolution of spin fields in continuum ferromagnets around the effective field $H_{\text{eff}}$,

$$m_t = -\alpha_1\, m \times (m \times H_{\text{eff}}) + \alpha_2\, m \times H_{\text{eff}}\,, \quad \alpha_1, \alpha_2 \geq 0\,, \tag{3.2}$$

where $m \equiv (m^1, m^2, m^3) : \omega \times (0,T) \to \mathbb{R}^3$, with $|\,m\,| = 1$, and $H_{\text{eff}} = -D\mathcal{E}_\alpha$, together with (1.4) and Maxwell's equation (1.1) in a quasi-static approximation. This equation linearly combines the heat flow of harmonic maps to the sphere $S^2$, $m_t = -m \times (m \times \Delta m)$, and the Schrödinger flow $m_t = m \times \Delta m$ in the case $\overline{H}_{\text{eff}} = \Delta m$.

Problem (3.2) is a strongly coupled degenerated quasi-linear parabolic system, which makes it hard to analyze mathematically. In order to understand the essential

properties of this phenomenological model describing nonequilibrium magnetism, we restrict ourselves to the exchange of energy contributions in the effective field, defining thus the reduced effective field $\overline{H}_{\text{eff}} = \Delta m$. Supposing classical solutions to (3.2) in this case, by using the identity $a \times (b \times c) = \langle a, c\rangle_{\mathbb{R}^3} b - \langle a, b\rangle_{\mathbb{R}^3} c$, we compute

$$m \times (m \times \Delta m) = \langle m, \Delta m\rangle_{\mathbb{R}^3} m - |\, m\,|^2 \Delta m\,.$$

In addition, if we multiply (3.2) by $m$, we find $\langle m, m_t\rangle_{\mathbb{R}^3} \equiv \frac{1}{2}\frac{d}{dt}|\, m\,|^2 = 0$, and hence $|\, m\,|^2 = 1$ everywhere in $\mathbb{R}^+ \times \omega$. Now, $m \cdot \nabla m = 0$, or $\langle m, \Delta m\rangle_{\mathbb{R}^3} = -|\, \nabla m\,|^2$, which is the reason for the following LLG equation:

$$m_t - \alpha_1 \Delta m = \alpha_1 |\, \nabla m\,|^2 m + \alpha_2\, m \times \Delta m \quad \text{in } \omega_T := (0,T) \times \omega\,, \tag{3.3}$$

$$\partial_n m = 0 \quad \text{on } \partial\omega_T := (0,T) \times \partial\omega\,, \tag{3.4}$$

$$m(0,x) = m_0(x) \quad \forall\, x \in \omega\,, \quad |\, m_0\,| = 1 \quad \text{a.e. in } \omega\,. \tag{3.5}$$

Note that the natural boundary condition resulting from the balance of torque, $m \times \partial_n m = 0$, can be simplified to (3.4) as $m \in S^2$. If (3.3) holds in a classical sense, an equivalent formulation would result from taking the cross-product with $m$ to replace the term scaled by $\alpha_2$,

$$\frac{\alpha_1}{\alpha_1^2+\alpha_2^2} m_t - \frac{\alpha_2}{\alpha_1^2+\alpha_2^2} m \times m_t = \Delta m + |\, \nabla m\,|^2 m \quad \text{in } \omega_T\,, \tag{3.6}$$

which is also known as the Gilbert equation [49]. By again using the above vector identity and $|\, m\,|^2 = 1$, we can recast (3.6) into the form

$$\frac{\alpha_2}{\alpha_1^2+\alpha_2^2} m_t + \frac{\alpha_1}{\alpha_1^2+\alpha_2^2} m \times m_t = m \times \Delta m \quad \text{in } \omega_T\,. \tag{3.7}$$

The choice between the Gilbert version and the Landau–Lifshitz version of the dynamic equation for magnetization is often based on mathematical convenience; both equations preserve the length of a smoothly varying magnetization vector and both can be studied in the framework of evolution problems of harmonic maps. The next example is taken from [90].

EXAMPLE 3.4. *In* [109] *the Landau–Lifshitz solution of Example* 2.1 *is generalized to the nonstationary case, where* $H_{\text{ext}} = -H\xi_3$ *is aligned to the easy axis and* $H < \frac{\alpha_1}{2\alpha_2}$ *constant is not too big. The traveling-wave solution found by Walker is*

$$\vartheta(x_1,t) = \arccos\left(\tanh\frac{x_1 - v_H t}{\delta_H}\right), \qquad \varphi(x_1,t) = \varphi_H\,,$$

*for fixed* $(\,\varphi_H, \delta_H, v_H\,)$ *given by*

$$\sin(2\varphi_H) = -\frac{2\alpha_2}{\alpha_1} H\,, \quad \delta_H = \sqrt{\frac{\alpha}{\beta + \sin^2(\varphi_H)}}\,, \quad v_H = H\frac{\alpha_1^2+\alpha_2^2}{\alpha_2}\sqrt{\frac{\alpha}{\beta+\sin^2(\varphi_H)}}\,.$$

*The solution supports the idea of a flat domain wall moving with velocity* $v_H$ *in the direction of the* $x_1$*-axis. Hence, crucial parameters which control the dynamics of a domain wall are its thickness* $w$ *and wall mobility* $\nu := \lim_{H\to 0}\frac{v_H}{H} = \frac{w(\alpha_1^2+\alpha_2^2)}{\alpha_2}$.

First existence results for the LLG equation in the presence of magnetostrictive effects are due to Visintin [106]; see also [5, 15]: locally existing solutions are globally extended thanks to the valid energy law; see below. In 1992, by a method introduced in [33] to prove nonuniqueness of weak solutions to the heat flow of harmonic

maps, Alouges and Soyeur [5] established a nonuniqueness result for weak solutions to problem (3.3)–(3.5) for $\omega \subset \mathbb{R}^3$; the idea was to take a singular solution of the type $g(\frac{x}{|x|})$ as the initial datum and then to show that there is another nonstatic solution emanating from such a datum. These earlier results do not discuss possible singularities of the solution; this question is addressed in a further study of weak solutions ("Struwe solutions") for domains $\omega \subset \mathbb{R}^2$ without boundary due to Guo and Hong [50]: these solutions are regular away from at most finitely many isolated points in $\omega_T$, and with decreasing energy; they are globally regular in the case of small initial energies. Their proof uses the intrinsic Liapunov structure of the problem and local energy arguments developed for harmonic maps by Struwe; see [101] for a survey. In the following, the study of the partial regularity of Struwe solutions [42] and their uniqueness [25] (cf. [54] for correcting remarks) again follows corresponding previous results in the harmonic mapping theory (1994, M. Feldman; 1995, Y. Chen, J. Li, and F.H. Lin; 2002, R. Moser on the partial regularity of the (constrained) Struwe's solution; 2004, C. Melcher on the partial regularity of Struwe's solution [78]; 1996, A. Freire on the uniqueness of Struwe's solution for the two-dimensional Cauchy problem). However, the possible development of finite-time (finite-energy) singularities is still an open problem for the LLG equation, thus motivating numerical studies [9]; see also Example 3.3.

DEFINITION 3.1. *A vector function* $\{m(t,x)\}$ *is said to be a global weak solution to* (3.6) *if* $m$ *is defined a.e. in* $\omega_T$ *such that*

1. $m \in L^\infty(0,\infty; H^1(\omega,\mathbb{R}^n))$ *and* $m_t \in L^2((0,\infty); L^2(\omega,\mathbb{R}^n))$,
2. $|\, m(t,x)\,|^2 = 1$ *a.e. on* $\mathbb{R}^+ \times \omega$,
3. (3.6) *holds in the sense of distributions,*
4. $m(0,x) = m_0(x)$ *in the sense of traces,*
5. *for all* $T > 0$,

$$\frac{1}{2} \| \nabla m(T) \|^2 + \frac{\alpha_1}{\alpha_1^2+\alpha_2^2} \int_0^T \| m_t(s) \|^2 \, \mathrm{d}s \le \frac{1}{2} \| \nabla m_0 \|^2 .$$

Verification of weak solutions to the LLG equation in higher dimensions requires a Ginzburg–Landau penalization strategy [50, 101], which defines a weak solution $m$ to the LLG equation as a suitable limit of $\{m^\varepsilon\}_{\varepsilon>0}$, where each element solves

$$\frac{\alpha_1}{\alpha_1^2+\alpha_2^2} m_t^\varepsilon - \frac{\alpha_2}{\alpha_1^2+\alpha_2^2} m^\varepsilon \times m_t^\varepsilon - \Delta m^\varepsilon + g(m^\varepsilon) = 0 \quad \text{in } \omega_T , \tag{3.8}$$

$$\frac{\partial m^\varepsilon}{\partial n} = 0 \quad \text{on } \partial\omega_T , \tag{3.9}$$

$$m^\varepsilon(0,x) = m_0^\varepsilon(x) \quad \forall\, x \in \omega , \quad |\, m^0\,| = 1 \quad \text{in } \omega \tag{3.10}$$

for $g(m^\varepsilon) = \nabla G(m^\varepsilon)$ and $G(m^\varepsilon) = \frac{1}{4\varepsilon^2}(|\, m^\varepsilon\,|^2 - 1)^2$; by standard Galerkin approximation, consider solutions $\{m^{\varepsilon,h}\}$ which satisfy the (semi)discrete energy identity

$$\frac{\alpha_1}{\alpha_1^2+\alpha_2^2} \int_0^T \| m_t^{\varepsilon,h}(s) \|^2 \, \mathrm{d}s + \frac{1}{2} \| \nabla m^{\varepsilon,h}(T) \|^2 + \int_0^T \int_\omega G(m^{\varepsilon,h}) \, \mathrm{d}x\mathrm{d}s = \frac{1}{2} \| \nabla m_0 \|^2 , \qquad h > 0 \ , \tag{3.11}$$

where $h$ is a mesh parameter. This result carries over to the limiting case $h \to 0$; moreover, by testing (3.8) with $m^\varepsilon - \frac{m^\varepsilon}{|\, m^\varepsilon\,|} \min\{1, |\, m^\varepsilon\,|\}$, one may show $|\, m^\varepsilon\,| \le 1$

a.e. on $\mathbb{R}^+ \times \omega$. Both ingredients now suffice to select convergent subsequences (not relabeled) $\{m^\varepsilon\}_\varepsilon$ such that

$$
\begin{aligned}
& m^\varepsilon \to m \quad \text{weakly* in } L^\infty\big(\mathbb{R}^+; H^1(\omega,\mathbb{R}^n)\big)\,,\\
& m_t^\varepsilon \to m_t \quad \text{weakly in } L^2\big(\mathbb{R}^+; L^2(\omega,\mathbb{R}^n)\big)\,,\\
& m^\varepsilon \times m_t^\varepsilon \to m \times m_t \quad \text{weakly in } L^2\big(\mathbb{R}^+; L^2(\omega,\mathbb{R}^n)\big)\,,\\
& m^\varepsilon \to m \quad \text{strongly in } L^2\big(\mathbb{R}^+; L^2(\omega,\mathbb{R}^n)\big)\,,\\
& |\,m\,| = 1 \quad \text{a.e. on } \mathbb{R}^+ \times \omega\,.
\end{aligned}
\tag{3.12}
$$

Finally, by taking the cross-product of (3.8) with $m^\varepsilon$, we can verify that the limit satisfies (3.6).

REMARK 3.1. *For the Cauchy problem $\omega = \mathbb{R}^3$, Alouges and Soyeur* [5] *use a finite-difference discretization of* (3.2) *($\tilde{H}_{\text{eff}} = \Delta m$) to derive the following ODE with Lipschitz-continuous right-hand side:*

$$
\partial_t m_h = -\alpha_1\, m_h \times (m_h \times \tilde{\Delta}_h m_h) + \alpha_2\, m_h \times \tilde{\Delta}_h m_h\,, \qquad m_h(0) = m_{0,h}.
$$

*This identity holds for all gridpoints, where $\tilde{\Delta}_h$ denotes the standard discrete Laplacian; conservation of $|\,m_h\,| = 1$ at every gridpoint and a semidiscrete energy law are the relevant steps to verify the existence of a weak solution in this context.*

REMARK 3.2. *An interesting approach to understanding wall dynamics is given in* [90]*, where a reduced sharp-interface model for their dynamics in hard ferromagnetic bodies is derived from the LLG equation by asymptotic analysis ($\beta \to \infty$). The idea of the construction is to asymptotically balance wall thickness, anisotropy effects, and wall mobility appropriately, leading to a limiting equation which describes the evolution of the flat domain wall by its mean curvature and a nonlocal forcing term.*

A crucial problem in the analysis of (3.2) is again the nonconvex constraint $|\,m\,| = 1$, which is penalized by the Ginzburg–Landau approximation (3.8); perturbation effects due to this strategy are then controlled by stability properties (i.e., energy law and $|\,m^\varepsilon\,| \le 1$) to eventually verify the convergence (3.12). Next to the strongly nonlinear character of the problem, proper dealing with the nonconvexity numerically is a problem since it cannot be satisfied a.e. anymore. Explicit time integrators of high order and occasional updates during the evolution to approximate $|\,m\,| = 1$ are the most commonly used strategies in the engineering literature [46], but they suffer from severe limitations with respect to admissible time-steps [44, 110] and nonreliable dynamics. From this perspective, recent developments in numerical micromagnetism aim at constructing efficient convergent schemes for the cases $H_{\text{eff}} = -D\mathcal{E}_\alpha$, both for $\alpha = 0$ and $\alpha > 0$. First results for the case $\alpha = 0$ in the more general framework of Maxwell–LLG have been done by Joly, Vacus, and Monk [58, 57, 83], addressing energy decay and conservation of length for iterates of their proposed schemes in the case of (known) smooth driving (electro)magnetic fields. Approaches are based on the given form (3.2) to easily detect these stability properties in the discrete setting. An interesting semidiscrete scheme to efficiently solve (3.2) is proposed in [29].

ALGORITHM 3.2.

1. *Let $m^{0,\ell} = m_0$ for $\ell \ge 0$.*
2. *For each $1 \le j \le J$, $1 \le \ell \le \ell_{j,\max}$, and $m^{j,0} = m^{j-1,\ell_{j-1,\max}}$, compute*

$m^{j,\ell} \in L^\infty(\omega, \mathbb{R}^n)$ *from*

$$d_t m^{j,\ell} = -\frac{\alpha_1}{4} \frac{m^{j,\ell}}{|\, m^{j,\ell}\,|} \times \Big( \big( m^{j-1,\ell-1} + m^{j,\ell-1} \big) \times \big( H_{\text{eff}}^{j-1,\ell-1} + H_{\text{eff}}^{j,\ell-1} \big) \Big) + \alpha_2\, m^{j,\ell} \times \big( H_{\text{eff}}^{j-1,\ell-1} + H_{\text{eff}}^{j,\ell-1} \big)\,.$$

3. *Stop iteration at level* $1 \le j \le J$ *in the case* $|\, m^{j,\ell} - m^{j,\ell-1}\,| \le k^\beta$, $\beta > 0$, *and set* $m^{j,\ell} = m^{j-1,\ell_{j-1,\max}}$.

For smooth $H_{\text{eff}} = -D\varphi + H$, $\beta \ge 3$, and $k \le k_0(t_J)$, this is a second-order convergent, length-preserving method [29]; in practice, $\max_j \ell_{j,\max} = 2$ is usually sufficient to meet the stopping criterion. In the remainder of this section we will focus on the case $\alpha > 0$.

**3.2.1. Discretization of Ginzburg–Landau Penalization (3.8)–(3.10).** In [88] Pistella and Valente numerically studied finite-time blow-up of solutions to the LLG equation subject to additional surface exchange contributions: for this purpose, they consider a fully discrete finite-difference version of the Ginzburg–Landau approximation ($\alpha_1, \alpha_2 \ge 0$)

$$m_t^\varepsilon - \alpha_1\, \Delta m^\varepsilon + \alpha_1 g(m^\varepsilon) = \alpha_2\, (m^\varepsilon \times \Delta m^\varepsilon) \quad \text{in } \omega_T\,, \tag{3.13}$$

$$\partial_n m^\varepsilon = 0 \quad \text{on } \partial\omega_T\,, \tag{3.14}$$

$$m^\varepsilon(0,x) = m_0(x) \quad \forall\, x \in \omega\,, \quad |\, m_0\,| = 1 \quad \text{in } \omega \tag{3.15}$$

for $g = \nabla G$, with $G(x) = \frac{1}{4\varepsilon^2}(x^2-1)^2$, which is based on the explicit Euler's method; by restricting the time-step $k > 0$ as ($\alpha_1 = \alpha_2 = 1$)

$$k \le \min\left[ \frac{\varepsilon^2 h^2}{2(\varepsilon^2 + h^2)}, \frac{h^2}{4} \right], \tag{3.16}$$

$\max_i |\, m_h^{\varepsilon,j}\,| \le 1$ and a discrete energy law corresponding to (3.11) are verified. These stability results are the key to verifing the convergence of a subsequence to solutions of (3.13)–(3.15) for every positive $\varepsilon > 0$ and finally of a subsequence to the weak solution of the limiting problem (3.3); see also [23] for blow-up studies using a stable, semi-explicit finite-difference scheme to discretize the limiting problem (3.7) directly.

Approximation of structures governed by the LLG equation requires small values of $\varepsilon > 0$ such that (3.16) severely restricts the values of time-steps $k > 0$. From this point of view, the following discretization of (3.8)–(3.10) is more flexible (cf., e.g., [45]): Given $m_{0,h} = P_h m_0$, find $m_h^j \in V_h(\omega; \mathbb{R}^n)$ for all $1 \le j \le J$ such that

$$\begin{aligned} &\frac{\alpha_1}{\alpha_1^2 + \alpha_2^2} \Big( d_t m_h^j, \phi_h \Big) + \Big( \nabla \overline{m}_h^{j-1/2}, \nabla \phi_h \Big) \\ &+ \frac{1}{2\varepsilon^2} \Big( (|\, m_h^j\,|^2 + |\, m_h^{j-1}\,|^2 - 2) \overline{m}_h^{j-1/2}, \phi_h \Big) = \frac{\alpha_2}{\alpha_1^2 + \alpha_2^2} \Big( m_h^{j-1} \times d_t m_h^j, \phi_h \Big)\,, \end{aligned} \tag{3.17}$$

where we denote $d_t \phi^j := k^{-1}\{\phi^j - \phi^{j-1}\}$ and $\overline{\phi}^{j-1/2} := \frac{1}{2}\{\phi^j + \phi^{j-1}\}$. Note that the right-hand term in (3.17) comes in a linear form, since $(\overline{m}_h^{j-1/2} \times d_t m_h^j, \phi_h) = (m_h^j \times d_t m_h^j, \phi_h)$. Consistency and the discrete energy law are desirable characteristics of (3.17) for the whole range of parameters $k, h, \varepsilon > 0$.

LEMMA 3.2. *The solution* $\{m_h^j\}_{j=1}^J$ *satisfies, for any* $k > 0$,

(i) $\max_{1\le j\le J} \| m_h^j \|_{L^\infty} \le 1\,,$

(ii) $\dfrac{\alpha_1}{\alpha_1^2+\alpha_2^2} k \sum_{j=1}^{J} \| d_t m_h^j \|^2 + \dfrac{1}{2} \max_{1\le j\le J} \| \nabla m_h^j \|^2 + \| G(m^j) \|_{L^1} = \dfrac{1}{2} \| \nabla m_{0,h} \|^2\,.$

*Proof.* Choosing $\phi_h = d_t m_h^j$ yields the result. ∎

**3.2.2. Approximation of Weak Solutions to the LLG Equation.** As outlined in section 3.2, so far it is not clear whether (3.2) also admits a finite-time singularity formulation. For this reason, it is convenient for reliable numerics for the LLG equation to deal with weak solutions. Verification of a corresponding discrete energy law for a discretization of the limiting problem (3.2) ($H_{\rm eff} = \Delta m$) is a challenging task: first, conservation of $|\,m\,| = 1$ rules out the implicit Euler method; second, spatial discretization using finite elements does not allow this nonconvex constraint to hold in a pointwise fashion.

EXAMPLE 3.5. *Given* $m_0 \in H^1(\omega, S^{n-1})$, *consider the implicit Euler method*

$$d_t m^j - \alpha_1 \Delta m^j = \alpha_1 |\,\nabla m^j\,|^2 m^j + \alpha_2\, m^j \times \Delta m^j \quad \text{in } \omega\,, \qquad \frac{\partial m^j}{\partial n} = 0 \quad \text{on } \partial\omega\,.$$

*We proceed by contradiction and suppose* $|\,m^{j-1}\,| = 1$ *a.e.: multiplication by* $m^j$ *yields*

$$d_t |\,m^j\,|^2 + k\,|\,d_t m^j\,|^2 = 0 \quad \text{for almost every } x \in \omega\,. \tag{3.18}$$

*Note that* $|\,m^j\,|^2 = 1$ *a.e. in* $\omega$ *is violated in general—in contrast to the continuous equation.*

We now propose two fully discrete, consistent schemes which satisfy a discrete energy law and hence allow for approximation of weak solutions to the LLG equation.

The first scheme uses lumped mass integration defined by

$$(\chi,\eta)_h = \sum_{K\in\mathcal{T}_h} \int_K I_h(\chi\eta)\,{\rm d}x \quad \forall\,\chi,\eta \in C(\overline{\omega})\,,$$

where $I_h : C(\overline{\omega}) \to V_h$ denotes the (linear) Lagrange interpolation operator on $\mathcal{T}_h$.

The following first consistent discretization of (3.2) was motivated by [11].

PROBLEM 3.1. *Given* $m_h^0 = I_h(m^0)$, *compute iterates* $m_h^j \in V_h(\omega;\mathbb{R}^n)$, $j \ge 1$, *from*

$$\begin{aligned}(d_t m_h^j, \phi_h)_h = &-\alpha_1\big(\overline{m}_h^{j-1/2} \times (\overline{m}_h^{j-1/2} \times \Delta_h \overline{m}_h^{j-1/2}), \phi_h\big)_h \\ &+ \alpha_2\big(\overline{m}_h^{j-1/2} \times \Delta_h \overline{m}_h^{j-1/2}, \phi_h\big)_h \quad \forall\,\phi_h \in V_h(\omega;\mathbb{R}^n)\,.\end{aligned}$$

Here, we denote $(-\Delta_h\phi_h, \mathfrak{Z}_h)_h = (\nabla\phi_h, \nabla\mathfrak{Z}_h)$. By Lipschitz continuity of the right-hand side, the problem has a unique solution. The following bounds verify $|\,m_h^j(x)\,| = 1$ for all vertices $x \in \mathcal{E}$, as well as the discrete energy law for (3.18) for every $k > 0$ and every $1 \le j \le J$:

(i) $|\,m_h^j(x)\,| = 1 \quad \forall\, x \in \mathcal{E}\,,$

(ii) $\dfrac{1}{2}\| \nabla m_h^J \|^2 + \alpha_1 k \sum_{j=1}^{J} \| \overline{m}_h^{j+1/2} \times \Delta_h \overline{m}_h^{j+1/2} \|^2 = \dfrac{1}{2}\| \nabla m_h^0 \|^2\,.$

Choose $\phi_h = \phi_i \overline{m}_h^{j-1/2}$, $\phi_i \in V_h(\omega, \mathbb{R}^2)$ such that $\phi_i(x_\ell) = \delta_{i\ell}$ to verify (i); assertion (ii) follows from selecting $\phi_h = -\Delta_h \overline{m}_h^{j-1/2}$. However, convergence toward weak solutions of (3.3)–(3.5) is an open problem.

Another discretization of the LLG equation is due to Alouges and Jaisson [4] and uses the Gilbert equation (3.7): if we take $\phi = m \times w$, where $w \in H^1(\omega_T, \mathbb{R}^3) \cap L^\infty(\omega_T, \mathbb{R}^3)$ satisfies $\langle w, m \rangle_{\mathbb{R}^3} = 0$ a.e. in $\omega$, we get

$$\frac{\alpha_1}{\alpha_2} \int_{\omega_T} \langle m_t, w \rangle_{\mathbb{R}^3} \, \mathrm{d}x\mathrm{d}t - \int_{\omega_T} \langle m \times m_t, w \rangle_{\mathbb{R}^3} \, \mathrm{d}x\mathrm{d}t = -\frac{\alpha_1^2 + \alpha_2^2}{\alpha_2} \int_{\omega_T} \langle \nabla m, \nabla w \rangle_{\mathbb{R}^9} \, \mathrm{d}x\mathrm{d}t \,, \tag{3.19}$$

from which the original weak formulation is re-obtained by taking $w = m \times \phi$ for any $\phi \in C_0^\infty(\omega_T, \mathbb{R}^n)$.

Now, consider the following subsets of $V_h(\omega; \mathbb{R}^n)$:

$$\mathcal{M}_h = \left\{ \phi_h \in V_h(\omega; \mathbb{R}^n) \middle| \, |\, \phi_h(x_\ell) \,| = 1 \ \forall\, x_\ell \in \mathcal{E} \right\},$$
$$\mathcal{F}_h^j = \left\{ \phi_h \in V_h(\omega; \mathbb{R}^n) \middle| \, \langle \phi_h(x_\ell), m_h^j(x_\ell) \rangle_{\mathbb{R}^3} = 0 \ \forall\, x_\ell \in \mathcal{E} \right\} \qquad \forall\, m_h^j \in \mathcal{M}_h \,.$$

A discretization of (3.19) could be obtained via the following Crank–Nicolson procedure: Let $m_h^0 = P_h m_0$. For $m_h^j \in \mathcal{M}_h$ given, find $m_h^{j+1} \in \mathcal{M}_h$ that solves, for all $w_h \in \mathcal{F}_h^{j-1}$,

$$\frac{\alpha_1}{\alpha_2}(d_t m_h^j, w_h) - (m_h^{j-1} \times d_t m_h^j, w_h) = -\frac{\alpha_1^2 + \alpha_2^2}{\alpha_2}(\nabla \overline{m}_h^{j-1/2}, \nabla w_h) \ . \tag{3.20}$$

Unfortunately, this latter equation is very difficult to solve because of the constraint on $m_h^j \in \mathcal{M}_h$. We therefore solve this equation only approximately and reconstruct $m_h^j$ in order to satisfy the constraint. The governing idea is to account for the fact that due to the constraint on $m_h^{j-1}$, $d_t m_h^j$ almost belongs to $\mathcal{F}_h^j$. Therefore, if we replace this term by a new unknown $v_h \in \mathcal{F}_h^{j-1}$, we may approximate (3.20) by

$$\frac{\alpha_1}{\alpha_2}(v_h, w_h) - (m_h^{j-1} \times v_h, w_h) = -\frac{\alpha_1^2 + \alpha_2^2}{\alpha_2}(\nabla \overline{m}_h^{j-1/2}, \nabla w_h) \quad \forall\, w_h \in \mathcal{F}_h^{j-1} \,. \tag{3.21}$$

The well-posedness of this problem follows from the fact that $v_h \in \mathcal{F}_h^{j-1}$ is determined by the difference of the continuous, positive symmetric bilinear form and a skew-symmetric continuous bilinear form. The algorithm in [4] now reads as follows.

ALGORITHM 3.3.

1. *Start with an initial magnetization* $m_h^0 \in \mathcal{M}_h$.
2. *Given* $m_h^{j-1} \in \mathcal{M}_h$, $1 \le j \le J$, *solve* (3.21) *and call* $v_h^{j-1} \in \mathcal{F}_h^{j-1}$ *the solution.*
3. *Compute* $m_h^j \in \mathcal{M}_h$ *from*

$$m_h^j(x) = \frac{m_h^{j-1}(x) + k v_h(x)}{|\, m_h^{j-1}(x) + k v_h(x) \,|} \quad \forall\, x \in \mathcal{E} \,.$$

A crucial step in the analysis of this discretization is to rewrite the second step in terms of $d_t m_h^j \in V_h(\omega; \mathbb{R}^n)$ and find the following characterization for all $w_h \in \mathcal{F}_h^{j-1}$:

$$\left| \frac{\alpha_1}{\alpha_2}(d_t m_h^j, w_h) - (m_h^{j-1} \times d_t m_h^j, w_h) + \frac{\alpha_1^2 + \alpha_2^2}{\alpha_2}(\nabla \overline{m}_h^{j-1/2}, \nabla w_h) \right| \le Ck \,\|\, w_h \,\|_{L^\infty} \,,$$

where $C$ does not depend on $j$ or $k$. Hence, this slightly perturbed version of (3.20) gives rise to the discrete energy inequality

$$\frac{\alpha_1}{\alpha_2} k \sum_{j=1}^{J} \| d_t m_h^j \|^2 + \frac{\alpha_1^2+\alpha_2^2}{\alpha^2} \max_{1\le j\le J} \| \nabla m_h^j \|^2 \le C t_J k + \frac{\alpha_1^2+\alpha_2^2}{\alpha^2} \| \nabla m_h^0 \|^2 .$$

This property eventually allows us to extract a convergent subsequence $\{m_{h'}^{j'}\}$ whose limit—first taken with respect to $k \to 0$ and then with respect to $h \to 0$—is a weak solution of the equation in Gilbert form (3.7). This program of convergence analysis for the above method is elaborated in [4]; current research specifies necessary requirements $F(k,h) \ge 0$ to ensure convergence [9] of the explicit scheme and also aims at constructing implicit, convergent discretizations which are exempted from these requirements [10].

**3.2.3. Approximation of Strong Solutions to the LLG Equation.** As outlined in the previous section, the provision of a consistent, discrete energy law to analytically determine convergence of computed iterates toward weak solutions is a nontrivial constraint for the construction of numerical methods to solve the LLG equation, and development in this direction is only very recent. Another direction of research in recent years is toward simple, easy-to-implement approximation schemes which perform remarkably well in practice: in general they do not satisfy a discrete energy law and tend to independently deal with the nonconvex algebraic constraint, nonlocality, and the evolutionary character of the problem in order to obtain efficient numerical schemes: splitting/projection schemes and penalization strategies.

In [43], a simple projection scheme is proposed to solve the LLG equation which is implicit and unconditionally stable; flexibility with respect to the choice of the time-step size is an important issue for a method to numerically resolve magnetic multiscale phenomena, which rules out time-explicit methods as possible efficient schemes. On the other hand, fully implicit schemes have to cope with the nonconvex, strongly nonlinear character of the problem; these are the main motivations to come up with the following scheme for (3.6).

ALGORITHM 3.4.

1. *Start with an initial discretization* $m_h^0 \in V_h(\omega;\mathbb{R}^n)$.
2. *Given* $m_h^{j-1} \in \mathcal{M}_h$, $1 \le j \le J$, *compute* $\tilde{m}_h^j \in V_h(\omega;\mathbb{R}^n)$ *for any* $j \ge 1$ *from*

$$\frac{\alpha_1}{\alpha_1^2+\alpha_2^2}\left(\frac{\tilde{m}_h^j - m_h^{j-1}}{k}, \phi_h\right) + (\nabla \tilde{m}_h^j, \nabla \phi_h)$$
$$- \frac{\alpha_2}{\alpha_1^2+\alpha_2^2}\left(m_h^{j-1} \times \frac{\tilde{m}_h^j - m_h^{j-1}}{k}, \phi_h\right) = 0 \quad \forall\, \phi_h \in V_h(\omega,\mathbb{R}^n) .$$

3. *Compute* $m_h^j \in \mathcal{M}_h$ *from* $m_h^j(x_\ell) = \frac{\tilde{m}_h^j(x_\ell)}{|\,\tilde{m}_h^j(x_\ell)\,|}$ *for all* $x_\ell \in \mathcal{E}$.

In order to efficiently handle nonlinear effects, the error analysis in [43] for the case of classical solutions to the LLG equation is based on a characterization of the solution by a nonlinear recursion relation; for simplicity, for the heat flow of harmonic maps (i.e., $\alpha_1 = 1$, $\alpha_2 = 0$), we find

$$m_h^j(x_\ell) = \frac{(\mathrm{Id} - k\Delta_h)^{-1} m_h^{j-1}(x_\ell)}{|\,(\mathrm{Id} - k\Delta_h)^{-1} m_h^{j-1}(x_\ell)\,|} ,$$

where it is understood that the Neumann boundary condition is imposed when inverting the given operator. The authors in [43] now use Strang's trick to construct a correction of the exact solution of the LLG equation for $\alpha_1 = 1$, $\alpha_2 = 0$:

$$m(x,t_j) = \frac{(\mathrm{Id} - k\Delta)^{-1} m(x,t_{j-1})}{|\,(\mathrm{Id} - k\Delta)^{-1} m(x,t_{j-1})\,|} + \mathcal{O}(k^2)\,, \tag{3.22}$$

which satisfies (3.22) to higher-order accuracy. The same strategy is then used to construct a second-order projection scheme, which is not obtained simply by keeping involved operators in step 2 and considering averages in time, but requires some further correction terms: step 2 is then replaced by

$$\begin{aligned}
&\frac{\alpha_1}{\alpha_1^2+\alpha_2^2}\left(\frac{\tilde m_h^j - m_h^{j-1}}{k}, \phi_h\right) + (\nabla \overline{m}_h^{j-1/2}, \nabla\phi_h) - \frac{\alpha_2}{\alpha_1^2+\alpha_2^2}\left(m_h^{j-1}\times\frac{\tilde m_h^j - m_h^{j-1}}{k}, \phi_h\right)\\
&= k^2\Big[\Big(\langle \nabla(|\,\nabla m_h^{j-1}\,|^2), \nabla m_h^{j-1}\rangle_{\mathbb{R}^3}\Big) + \frac{1}{2}\Big(|\,\nabla m_h^{j-1}\,|^2[(\mathrm{Id} + m_h^{j-1}\times)^{-1} - \mathrm{Id}]\Delta_h m_h^{j-1}, \phi_h\Big)\Big].
\end{aligned}$$

Computational experiments are reported in [43] for the case of a heat-flow harmonic map to illustrate the unconditional stability of these projection strategies, but also to indicate an increase with respect to computational effort in the case of higher-order projection methods.

A slightly modified numerical strategy is studied in [93] for (3.3)–(3.5), where the Lagrange multiplier of the LLG equation is still kept in the discretization; the projection step then balances the damping character of the implicit Euler method; cf. Example 3.5.

ALGORITHM 3.5.

1. *Start with an initial discretization* $m_h^0 \in V_h(\omega;\mathbb{R}^n)$.
2. *Given* $m_h^{j-1} \in \mathcal{M}_h$, *compute* $m_h^j \in V_h(\omega;\mathbb{R}^n)$ *for any* $1 \le j \le J$ *from*

$$\begin{aligned}
&\left(\frac{\tilde m_h^j - m_h^{j-1}}{k}, \phi_h\right) + \alpha_1\,(\nabla \tilde m_h^j, \nabla\phi_h)\\
&= \alpha_1\left(|\,\nabla \tilde m_h^{j-1}\,|^2 \tilde m_h^j, \phi_h\right) - \alpha_2\left(\tilde m_h^j \times \nabla \tilde m_h^j, \nabla\phi_h\right) \quad \forall\,\phi_h \in V_h(\omega,\mathbb{R}^n)\,.
\end{aligned}$$

3. *Compute* $m_h^j \in \mathcal{M}_h$ *from* $m_h^j(x_\ell) = \frac{\tilde m_h^j(x_\ell)}{|\,\tilde m_h^j(x_\ell)\,|}$ *for all* $x_\ell \in \mathcal{E}$.

By replacing all quantities in step 2 by tilted ones, we arrive at the following penalized discretized LLG equation:

$$\begin{aligned}
&(d_t \tilde m_h^j, \phi_h) + \alpha_1(\nabla \tilde m_h^j, \nabla\phi_h) + \frac{1}{\varepsilon}\left(\tilde g(\{\tilde m_h^j\}), \phi_h\right)\\
&\qquad = \alpha_1\left(|\,\nabla \tilde m_h^{j-1}\,|^2 \tilde m_h^j, \phi_h\right) - \alpha_2\left(\tilde m_h^j \times \nabla \tilde m_h^j, \nabla\phi_h\right),
\end{aligned} \tag{3.23}$$

where $\varepsilon = k$ and $\tilde g(\{\tilde m_h^j\}) = \big(1 - \frac{1}{|\,\tilde m_h^{j-1}\,|}\big)\tilde m_h^{j-1}$. Hence, the projection scheme above corresponds to a semi-explicit penalization with a new penalization function, which is additionally introduced to the discretization of the LLG equation to enforce $|\,m_h^j(x_\ell)\,| = 1$ for all $x_\ell \in \mathcal{E}$. The following error estimates are verified in [93] for (3.23) in the case of quasi-uniform triangulations of $\omega \subset \mathbb{R}^2$ and related numerical

scales $k^{-1/2} = o(h^{-1})$:

$$\max_{0\le j\le J} \| m(t_j) - m_h^j \| + \left( k \sum_{j=1}^{J} \| \nabla (m(t_j) - m_h^j) \|^2 \right)^{1/2}$$

$$+ \left( \frac{k}{\varepsilon} \sum_{j=1}^{J} \Big[ \| m(t_j) - m_h^j \|_{L^4}^4 + \| \langle m(t_j) - m_h^j, m(t_j) \rangle_{\mathbb{R}^3} \|^2 \Big] \right)^{1/2} \le C(k+h)\,. \tag{3.24}$$

The proof of this result uses an inductive argument to compensate for the lack of a discrete energy law, invoking (i) the existence of (locally verifiable) strong solutions to the LLG equation, in combination with (ii) the above approximation results and given restrictions on meshes and numerical scalings, in particular. These arguments and results have been extended to cases $\omega \subset \mathbb{R}^3$ in [30].

The connection between projection schemes and (semi-explicit) penalization ansatzes to enforce numerically the nonconvex constraint is the reason for the study of other strategies $\tilde{g} \equiv \tilde{g}_i$, $i = 1, 2, 3$:

$$\tilde{g}_1(\{\tilde{m}_h^j\}) = (|\, \tilde{m}_h^{j-1} \,|^2 - 1)\tilde{m}_h^j\,, \quad \tilde{g}_2(\{\tilde{m}_h^j\}) = \left(1 - \frac{1}{|\, \tilde{m}_h^{j-1} \,|}\right) \tilde{m}_h^j\,,$$

$$\tilde{g}_3(\{\tilde{m}_h^j\}) = \left(1 - \frac{1}{|\, \tilde{m}_h^{j-1} \,|^{2-\gamma}}\right) \tilde{m}_h^j, \quad \gamma \in \mathbb{N}_0\,.$$

Studies in [93] show that $\varepsilon^{-1} = o(k^{-1})$ is a stable choice for $\tilde{g}_1$, leading to optimal convergence behavior; computational experiments show suboptimal behavior in the case where $\varepsilon < k$ is chosen. Moreover, choosing $\gamma \in \mathbb{N}_0$ large yields a better balancing of stability and accuracy requirements, where the choice of $\varepsilon$ is more flexible with respect to the time-step size $k$. These results evidence replacement of the projection method above by a "scaled projection method," parameterized by $\gamma \in \mathbb{N}$; see Figure 2.4(d).

ALGORITHM 3.6.

1. *Start with an initial discretization* $m_h^0 \in V_h(\omega, \mathbb{R}^n)$.
2. *Given* $\tilde{m}_h^{j-1}, m_h^{j-1} \in V_h(\omega; \mathbb{R}^n)$, $1 \le j \le J$, *compute* $\tilde{m}_h^j \in V_h(\omega; \mathbb{R}^n)$ *from*

$$\left( \frac{\tilde{m}_h^j - m_h^j}{k}, \phi_h \right) + \alpha_1 \left( \nabla \tilde{m}_h^j, \nabla \phi_h \right)$$
$$= \alpha_1 \left( |\, \nabla \tilde{m}_h^{j-1} \,|^2 \tilde{m}_h^j, \phi_h \right) - \alpha_2 \left( \tilde{m}_h^j \times \nabla \tilde{m}_h^j, \nabla \phi_h \right) \quad \forall\, \phi_h \in V_h(\omega, \mathbb{R}^n)\,.$$

3. *Compute* $m_h^j \in V_h(\omega; \mathbb{R}^n)$ *from* $m_h^j(x_\ell) = \frac{\tilde{m}_h^j(x_\ell)}{|\, \tilde{m}_h^j(x_\ell) \,|^{2-\gamma}}$ *for all* $x_\ell \in \mathcal{E}$.

So far, the magnetostatic stray field, anisotropy, and exterior magnetic fields which contribute in the model (3.2), (1.4) have been neglected, since they do not lead to further analytical problems in the general model; however, an efficient numerical treatment of the general model is not so evident and is studied in [93], where different contributions

$$H_{\mathrm{eff},1;h}^{j+1} = \alpha \Delta_h m_h^{j+1}\,, \qquad H_{\mathrm{eff},2;h}^{j} = -D\varphi(m_h^j) - \nabla u_h^j + H^{j+1}$$

are shifted in time to eventually account for $H_{\mathrm{eff},h}^{j+1} = H_{\mathrm{eff},1;h}^{j+1} + H_{\mathrm{eff},2;h}^{j}$ in the LLG equation; computed iterates $(\, u_h^j, m_h^j \,) \in V_h(\Omega) \times V_h(\omega; \mathbb{R}^n)$ again satisfy (3.24).

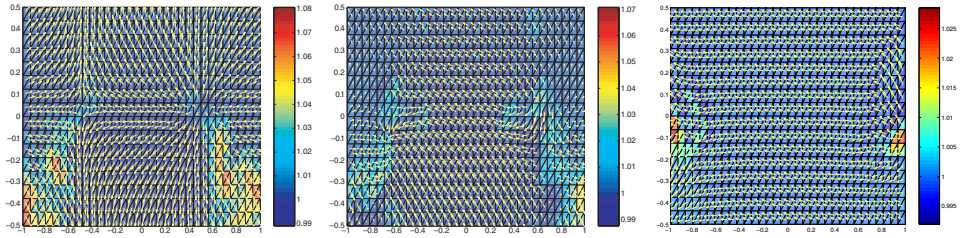

**Fig. 3.2** *Plot of magnetization $\tilde{m}_h^j$ and its modulus at subsequent times, using Algorithm* 3.7 *(from* [93]*).*

ALGORITHM 3.7.

1. *Start with* $(m_h^0, u_h^0)$*, where* $u_h^0 = \Delta_{\Omega,h}^{-1}\mathrm{div}_h(\chi_\omega m_h^0)$.

2. *Given* $(\tilde{m}_h^{j-1}, m_h^{j-1}, u_h^{j-1}) \in V_h(\omega,\mathbb{R}^n) \times V_h(\omega;\mathbb{R}^n) \times V_h^0(\Omega)$*,* $1 \le j \le J$*, compute* $\tilde{m}_h^j \in V_h(\omega,\mathbb{R}^n)$*, with* $\partial_n \tilde{m}_h^j = 0$ *on* $\partial\omega$*, for any* $j \ge 1$*, and* $\phi_h \in V_h(\omega,\mathbb{R}^n)$ *from*

$$\begin{aligned}&\left(\frac{\tilde{m}_h^j - m_h^{j-1}}{k}, \phi_h\right) + \alpha_1\alpha\big(\nabla\tilde{m}_h^j, \nabla\phi_h\big)\\ &= \alpha_1\alpha\big(|\nabla\tilde{m}_h^{j-1}|^2\tilde{m}_h^j, \phi_h\big) + \alpha_2\big(\nabla(\phi_h \times \tilde{m}_h^{j-1}), \nabla\tilde{m}_h^j\big)\\ &\quad + \alpha_2\big(m_h^{j-1} \times H_{\mathrm{eff},2;h}^{j-1}, \phi_h\big) - \alpha_1\big(m_h^{j-1} \times (m_h^{j-1} \times H_{\mathrm{eff},2;h}^{j-1}), \phi_h\big)\,.\end{aligned}$$

3. *Given* $\gamma \in \mathbb{N}_0$*, compute* $m_h^j \in V_h(\omega;\mathbb{R}^n)$ *from* $m_h^j(x_\ell) = \frac{\tilde{m}_h^j(x_\ell)}{|\tilde{m}_h^j(x_\ell)|^{2-\gamma}}$ *for all* $x_\ell \in \mathcal{E}$.

4. *Given* $\omega \Subset \Omega \subset \mathbb{R}^n$*, compute* $u_h^{j+1} \in V_h(\Omega)$ *from*

$$(\nabla u_h^{j+1}, \nabla w_h) = (m_h^{j+1}, \nabla w_h) \qquad \forall\, w_h \in V_h^0(\Omega)\,.$$

The following example is taken from [93].

EXAMPLE 3.6. *Let* $\omega = (-1,1)\times(-0.5,0.5)$*,* $H = (-100,0,0)$*, and* $e = -\frac{1}{\sqrt{2}}(1,1,0)$*, and fix parameters* $\alpha_1 = \alpha_2 = \alpha = \beta = 1$*,* $\Omega = (-4,4)^2$ *in* (3.2)*,* (1.4) *to evolve*

$$m_0 = \frac{\hat{m}}{\sqrt{|\hat{m}|^2 + \eta^2}} \quad \text{in } \omega\,, \qquad \hat{m}(x,y) = (x^2 + y^2 - \frac{1}{4}, y, 0)$$

*for* $\eta = 0.2$ *according to Algorithm* 3.7*. Snapshots which show the growing alignment of magnetization to the applied field* $H$ *are displayed in Figure* 3.2.

**3.2.4. Effective Dynamics of Soft Ferromagnetic Thin Films.** The dynamics of ferromagnetics is severely constrained in a thin film $\omega = \omega' \times (0,\delta) \subset \mathbb{R}^3$, leading to different behavior compared to bulk media. In [48], García-Cervera and E derived an effective dynamical equation for a soft ferromagnetic thin film in situations where $\alpha, \beta, |H_{\mathrm{ext}}| = \mathcal{O}(\delta)$, $\alpha_2 = 1$, and $\delta \ll \alpha_1$; moreover, to leading order it is plausible to ask for order parameters $m'(x') = (m_1'(x'), m_2'(x'))$ such that $|m'| = 1$ a.e. Then, by asymptotic analysis with respect to $\delta \to 0$, the spin dynamics for the limiting case is controlled by

$$m_t' = \left(\frac{1}{\alpha_1} + \alpha_1\right)\left(\tilde{H}_{\mathrm{eff}} - \langle m', \tilde{H}_{\mathrm{eff}}\rangle_{\mathbb{R}^2} m'\right), \tag{3.25}$$

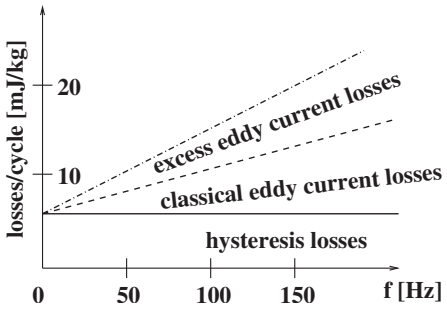


**Fig. 3.3** *Frequency dependence of different kinds of losses in a transformer steel* [55].

where $\tilde{H}_{\rm eff} = -D\mathcal{E}_{\rm thin}$ is now computed from

$$\mathcal{E}_{\rm thin}(m') = \alpha \int_\omega |\, \nabla m' \,|^2 \,{\rm d}x' + \int_\omega \varphi(m') \,{\rm d}x' - \int_\omega \langle H, m' \rangle_{\mathbb{R}^2} \,{\rm d}x' + \frac{1}{4} \,\| \,{\rm div}' \, m' \,\|^2_{H^{-1/2}(\Omega')} \,, \qquad \omega' \Subset \Omega' \subseteq \mathbb{R}^2 \,.$$

Computational comparisons of (3.25) with the full LLG equation show very good agreement in the regime $\delta \leq \alpha_1$ ($\alpha_2 = 1$) (cf. [48]); note that (3.25) for $\tilde{H}_{\rm eff} = \alpha \Delta m$ yields the heat flow of harmonic maps.

At first glance, it is surprising that the gyromagnetic term of the LLG equation in the thin film limit only contributes as a damping term for the in-plane components of $m$, moreover with a much larger damping coefficient $\frac{1}{\alpha_1}$. The reason for this is the requirement $\delta \ll \alpha_1$ that exchange mechanisms dominate all other geometric and physical parameters; unfortunately, this crucial constraint excludes reliable studies of dynamics, e.g., vortex dynamics, by using the reduced model (3.25) for practically relevant studies; cf. [44].

**3.3. A Mesoscopic-Level Model.** For mesoscale ferromagnets, the main interest lies in the evolution of averaged magnetizations rather than detailed, complex spin dynamics. The phenomenological model introduced by Roubíček and Kružík in [97, 98] combines the tendency to minimize Landau–Lifshitz energy during evolution with a rate-independent maximum-dissipation mechanism during magnetization switching from one pole to the other. In fact, there are many contributions to energetic losses if a ferromagnet is exposed to a switching external magnetic field. Besides hysteresis losses, which are independent of an external field frequency and which we are going to model here, there are also intrinsic damping, disaccommodation, and eddy currents; see Figure 3.3. Except for hysteresis losses, all others are rate dependent; we refer to [55] for more details. In this sense, hysteresis losses are considered as a limit for frequencies tending to zero. On the other hand, for ferromagnets, rate-independence holds with a good approximation in a fairly wide range of frequencies. Recently, this model was used to study an optimal control of a magnetization as a mathematical program with evolutionary equilibrium constraints; cf. [63].

**3.3.1. Rate-Independent Dissipation.** For the usual loading regimes and magnetically hard materials, one must consider a certain dissipation mechanism, which may also be influenced by impurities in the material without substantially affecting the stored energy. Hence, energy storage and dissipation mechanisms are, to some

extent, independent of each other, and, as the dissipation mechanisms are determined on an atomistic level, it seems that the only efficient way to incorporate them in a higher-level model is a phenomenological approach.

Our simplified standpoint is that the amount of dissipated energy within the phase transformation from one pole to the other can be described by a single, phenomenologically given number (of dimension $\mathrm{J/m^3} = \mathrm{Pa}$) depending on the coercive force $H_c$ [26]. Hence, we need to identify the particular poles according to the magnetization vector. Inspired by [80, 82] and considering $L$ poles ($L = 2$ for uniaxial magnets or $L = 6$ or 8 for cubic magnets), we define a continuous mapping $\mathfrak{L} : S^{n-1} \to \triangle_L$, where $\triangle_L := \{\xi \in \mathbb{R}^L;\ \xi_i \geq 0,\ i = 1, \dots, L,\ \sum_{i=1}^L \xi_i = 1\}$. In other words, $\{\mathfrak{L}_1, \dots, \mathfrak{L}_L\}$ forms a partition of unity on $S^{n-1}$ such that $\mathfrak{L}_i(s)$ is equal to one, if $s$ is in the $i$th pole, i.e., $s \in S^{n-1}$ is in a neighborhood of the $i$th easy-magnetization direction. Also, $\mathfrak{L}(m)$ in the (relative) interior of $\triangle_L$ indicates $m$ in the region where no definite pole is specified. Hence, $\mathfrak{L}$ plays the role of an order parameter.

In terms of the mesoscopic microstructure described by the Young measure $\nu$, the "mesoscopic" order parameter is naturally defined as

$$\varsigma = \Lambda\nu := \mathfrak{L} \bullet \nu,$$

where $[\mathfrak{L} \bullet \nu](x) := \int_{S^{n-1}} \mathfrak{L}(s)\nu_x(\mathrm{d}s)$. Thus, $\Lambda$ is just a continuous extension of the mapping $m \mapsto \mathfrak{L}(m)$, i.e., if $\{m_k\}$ converges to $\nu$ weakly* in $L^\infty(\omega; \mathbb{R}^n)$, then $\mathfrak{L}(m_k) \rightharpoonup \Lambda\nu$ weakly* in $L^\infty(\omega; \mathbb{R}^L)$.

In order to phenomenologically describe dissipative energetics, one must prescribe a potential of dissipative forces as a function of the rate of $\varsigma$. For rate-independent processes, this potential must be convex and homogeneous of degree one. Considering a norm $|\cdot|_{\mathbb{R}^L}$ on $\mathbb{R}^L$, one can postulate $\varrho(\dot\varsigma) = H_c|\dot\varsigma|_{\mathbb{R}^L}$. The energy density needed to transform the $i$th pole to the $j$th pole is then $H_c|e_i - e_j|_{\mathbb{R}^L}$, with $e_i$ the unit vector with one at the $i$th position.

In the following, we represent magnetization at time $t \geq 0$ by the couple $q = q(t) \equiv (\nu, \varsigma) = (\{\nu_{x,t}\}_{x\in\omega}, \varsigma(\cdot, t))$. Let us denote by $\mathcal{Q}$ the convex set of admissible configurations:

$$\begin{aligned}\mathcal{Q} := \Big\{ q = (\nu, \varsigma) \in L^\infty_{\mathrm{w}}\big(\omega; \mathcal{M}(S^{n-1})\big) \times L^\infty(\omega, \mathbb{R}^L) \big|\, \varsigma(x) \in \triangle_L\,, \\ \Lambda\nu = \varsigma \text{ for almost all } x \in \omega \Big\}.\end{aligned} \tag{3.26}$$

Let $\mathcal{G}(t, q) := \overline{\mathcal{E}}_0(q) - \langle F(t), q\rangle$ denote the Gibbs energy, where $\langle F(t), q\rangle = \langle \nu, H(t) \otimes \mathrm{Id}\rangle$, and $\mathcal{D}(q_1, q_2) := H_c \int_\omega |\,\varsigma_1 - \varsigma_2\,|_{\mathbb{R}^L}\,\mathrm{d}x$ denote the distance between two configurations $q_i = (\nu_i, \varsigma_i)$, $i = 1, 2$. In this way $F$ is the so-called generalized force. The general framework of Mielke, Theil, and Levitas [80, 81, 82] is used in the following to obtain a mesoscopic ferromagnetic model with appropriate solvability properties.

DEFINITION 3.3. *A process $q = q(t)$ is called stable if for all $t \in [0, T]$,*

$$\mathcal{G}(t, q) \leq \mathcal{G}(t, \tilde q) + \mathcal{D}\big(q, \tilde q\big) \quad \forall\, \tilde q \in \mathcal{Q}\,.$$

An important notion is the set of stable states $S(t)$ at time $t \geq 0$:

$$S(t) = \Big\{ q \in \mathcal{Q} \big|\ \mathcal{G}(t, q) \leq \mathcal{G}(t, \tilde q) + \mathcal{D}(q, \tilde q) \quad \forall\, \tilde q \in \mathcal{Q} \Big\}.$$

DEFINITION 3.4. *A process $q = q(t)$ satisfies the energy inequality if for all $s, t \in [0,T]$ such that $s \le t$,*

$$\underbrace{\mathcal{G}\big(t, q(t)\big)}_{\substack{\text{effective Gibbs}\\ \text{energy at time } t}} + \underbrace{\mathrm{Var}(\mathcal{D}, q; s, t)}_{\substack{\text{dissipated}\\ \text{energy}}} \le \underbrace{\mathcal{G}\big(s, q(s)\big)}_{\substack{\text{Gibbs energy}\\ \text{at time } s}} - \underbrace{\int_s^t \Big\langle \frac{\mathrm{d}F}{\mathrm{d}t}(\theta), q(\theta) \Big\rangle \,\mathrm{d}\theta}_{\substack{\text{reduced work of}\\ \text{external field}}} ,$$

*where the total variation over the time interval $[s,t]$ is defined in a standard way, without explicitly using any time derivative, as $\mathrm{Var}(\mathcal{D}, q; s, t) := \sup \sum_{j=1}^{J} \mathcal{D}\big(q(t_{j-1}), q(t_j)\big)$, where the supremum is taken over all $J \in \mathbb{N}$ and over all partitions of $[s,t]$ in the form $s = t_0 < t_1 < \cdots < t_{J-1} < t_J = t$.*

It was shown in [81] that in qualified cases the stability and energy inequality can be written in the form of a doubly nonlinear evolutionary inclusion

$$\partial R(q_t) + D\overline{\mathcal{E}_0}(q) + N_{\mathcal{Q}}(q) \ni F(t)\,, \quad q(0) = q_0\,, \tag{3.27}$$

where $q_0 = (\,\nu_0, u_0\,) \in \mathcal{Q}$ denotes the initial configuration, $N_{\mathcal{Q}}$ the normal cone to $\mathcal{Q}$ at $q$, and $\partial R$ the subdifferential of the energy $R(q) = \int_\omega \varrho(\varsigma)\,\mathrm{d}x = \int_\omega H_{\mathrm{c}}|\varsigma|_{\mathbb{R}^L}\,\mathrm{d}x$, which is dissipated during the transformation process. The advantage of defining a solution using Definition 3.5 is the absence of any time derivative and purely energetic considerations. In this sense, it can be seen as a weak form of (3.27).

DEFINITION 3.5. *The process $q = q(t)$, $q \equiv (\,\nu, \varsigma\,)$, will be considered a solution if $\nu \in L^\infty_{\mathrm{w}}\big(\omega_T; \mathcal{M}(S^{n-1})\big)$, $\varsigma \in BV\big([0,T]; L^1(\omega; \mathbb{R}^L)\big)$, and $q(t) \in \mathcal{Q}$ for all $t \in [0,T]$, and is stable for all $t \in [0,T]$ and satisfies the energy inequality in Definition* 3.4 *for all $s, t \in [0,T]$ such that $s \le t$.*

The existence of a solution satisfying this definition was shown in [97]. The Gibbs energy needs a slight regularization by a higher-order term, however.

REMARK 3.3. *By the reduced work in Definition* 3.4*, we mean (up to a sign) the usual work, i.e., $\int_s^t \langle F, \frac{\mathrm{d}q}{\mathrm{d}t}\rangle\,\mathrm{d}\theta$, but reduced by $\langle F(s), q(s)\rangle - \langle F(t), q(t)\rangle$, which is just the gap between the Gibbs and Helmholtz energies at time instances* 0 *and $t$.*

**3.3.2. Incremental Problems.** The existence of a response $t \mapsto q(t)$ with the above-mentioned properties was shown in an even more general case in [98] by a semidiscretization in time using the implicit Euler scheme. For simplicity, let us consider an equidistant partition of the time interval $[0,T]$ with a time-step $k > 0$, assuming $T/k$ an integer.

ALGORITHM 3.8. *Let $q^0 = q_0$. Find $q^j := \mathrm{argmin}_{q \in \mathcal{Q}} I(q)$ for $j = 1, \ldots, \frac{T}{k}$ and*

$$I(q) := \mathcal{G}(jk, q) + \mathcal{D}(q^{j-1}, q)\,.$$

If a global minimizer to this problem is not unique, then we just identify an arbitrary one as $q^j$. Then we define the piecewise constant interpolation $q \in L^\infty\big(0,T; L^\infty_{\mathrm{w}}(\omega; \mathcal{M}(S)) \times L^\infty\big(\omega; \mathbb{R}^L\big)$ as $q|_{((j-1)k, jk]} = q^j$ for $j = 1, \ldots, T/k$, and $q_k(0) = q^0$. A proof of the existence of a solution to the evolutionary problem can be found in [98]. It is based on the above incremental formulation and on a suitable limiting procedure.

**3.3.3. Numerical Solution.** A straightforward numerical approximation based on the incremental formulation in Algorithm 3.8 copes with the nonsmoothness of the dissipative term. However, in specific cases, using an approach from [65, 97], we can reformulate the problem as a smooth one with a few additional constraints and variables. One such situation is, e.g., if $L = 2$, $|b|_L = 2\max(|b_1|, |b_2|)$ for any

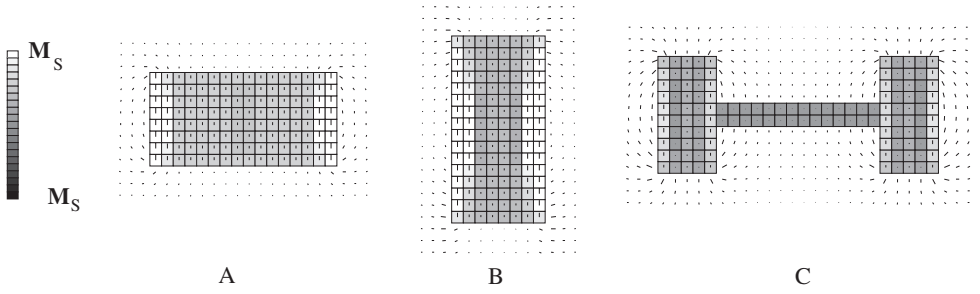


**Fig. 3.4** *Magnetization $m_h$ for two-dimensional cross sections of various bulk specimens computed from Algorithm* 3.9 *(also the surrounding demagnetizing field), displayed at specific times (after* [71]*).*

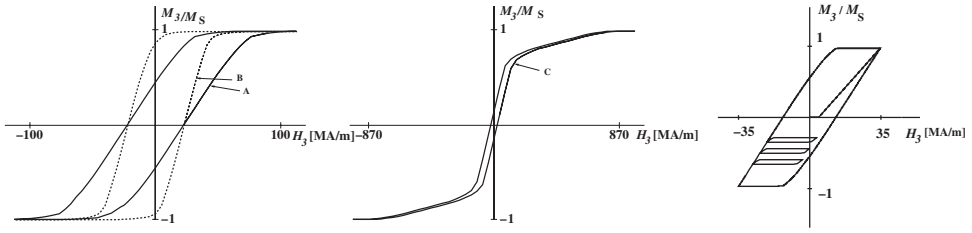


**Fig. 3.5** *Hysteresis loops corresponding to specimens* A, B, C *in Figure* 3.4 *(left, middle); virgin magnetization and minor hysteresis loops due to spatially varying activation threshold resulting from inhomogeneities of the magnetization process (after* [71, 72]*).*

$b \in \mathbb{R}^2$. Then $\varsigma(x) = \int_{S^{n-1}} s_3 \, \nu_x(\mathrm{d}s)$, where $s = (\, s_1, s_2, s_3 \,)$, or $\varsigma = m_3$, i.e., the third component of the magnetization. The stray field energy is calculated using the Green's function of the Laplace operator as described in [76, 75].

ALGORITHM 3.9. *Given $q^0 = q(0)$, for $j \le T/k$ compute*

$$(\, q^j, a^j \,) = \mathrm{argmin}_{\mathcal{Q} \times L^1(\omega)} J(q, a),$$

*where*

$$J(q, a) := \mathcal{G}(jk, q) + \int_\omega a(x) \, \mathrm{d}x \tag{3.28}$$

*and*

$$\begin{cases} H_{\mathrm{c}}(\int_{S^{n-1}} s_3 \nu_x^{k-1}(\mathrm{d}s) - \int_{S^{n-1}} s_3 \nu_x(\mathrm{d}s)) \le a(x) \text{ for almost all } x \in \omega \,, \\ H_{\mathrm{c}}(\int_{S^{n-1}} s_3 \nu_x(\mathrm{d}s) - \int_{S^{n-1}} s_3 \nu_x^{k-1}(\mathrm{d}s)) \ge -a(x) \text{ for almost all } x \in \omega \,. \end{cases}$$

It can be shown (see [65]) that Algorithms 3.8 and 3.9 are equivalent to each other in the sense that given a solution to either of them we can easily construct a solution to the other one. Algorithm 3.9 can be discretized in the same way as (2.4). Figures 3.4 and 3.5 display the magnetization, the surrounding stray field, and the resulting hysteresis loops for a uniaxial material CoZrDy at the temperature 4.2 K, using Algorithm 3.9. In the case that the mesoscopic order parameter $\varsigma$ is an affine function of the magnetization, one can rule out the Young measure from Definition 3.4. The resulting incremental problem is then formulated only in terms of

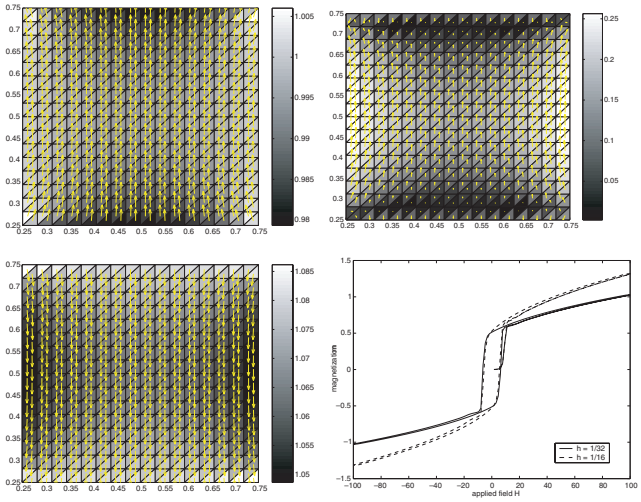


**Fig. 3.6** *Magnetization* $\{m_h^j\}_j$ *computed from Algorithm* 3.10 *close to first switching time at three subsequent time-steps, and corresponding hysteresis loop (after* [70]*).*

the magnetization; one has to replace the anisotropy density $\varphi$ by $\varphi^{**}$, however, and ends up with

$$\partial R^{**}(m_t) + D\tilde{\mathcal{E}}_0(m) + N_{\tilde{\mathcal{A}}}(m) \ni H\,, \qquad m(0) = 0\,,$$

where $R^{**}(m_t) := H_c \int_\omega |\,\varsigma(m_t)\,|\,\mathrm{d}x$; cf. (2.3)–(2.4). A discretization of this problem (in regularized form, $\gamma > 0$) using the implicit Euler method on an equidistant mesh $I_k = \{t_j\}_j$ leads to a convex problem at every time-step (compare to Problem 2.1).

ALGORITHM 3.10.

1. *Start with* $m_h^0 = P_h m^0 \in W_h(\omega;\mathbb{R}^2)$ *and fix* $k, h, \gamma > 0$.
2. *For each* $1 \le j \le J$, *find* $(\,m_h^j, u_h^j\,) \in W_h(\omega;\mathbb{R}^2) \times \tilde{V}_h^0(\Omega)$ *that satisfy*

$$(\nabla_h u_h^j, \nabla_h w_h) = (m_h^j, \nabla_h w_h) \quad \forall\, w_h \in \tilde{V}_h^0(\Omega)\,,$$

$$\nabla_h u_h^j + D\varphi^{**}(m_h^j) + H_c\,\mathrm{sgn}_\gamma\Big(\varsigma(m_h^j) - \varsigma(m_h^{j-1})\Big) D\varsigma(m_h^j) + \lambda_h^j m_h^j = P_h H^j \qquad \textit{a.e. in } \omega\,,$$

$$\lambda_h^j = \varepsilon^{-1}\frac{(\,|\,m_h^j\,| - 1)_+}{|\,m_h^j\,|} \qquad \textit{a.e. in } \omega.$$

This algorithm was studied in [70, 47], which motivates $\varepsilon = \mathcal{O}(h)$ and, in particular, $\gamma = \mathcal{O}(h^2)$; cf. Figure 3.6.

REMARK 3.4. *The mesoscopic model described above does not allow for modeling a virgin magnetization curve, i.e., the curve describing the evolution of the magnetization from a completely demagnetized specimen (i.e.,* $|\,m\,| = 0$ *in* $\omega$*) to the saturation state (*$|m| = 1$ *in* $\omega$*). The reason is that the coercive force* $H_c$ *is kept constant. One way to generalize the model so that it describes virgin magnetization processes is to make the coercive force dependent on the history of the magnetization. This idea was scrutinized in* [72, 98].

**4. Outlook.** The mathematical modeling of ferromagnetic materials has been a very active area of research for decades, and many important questions raised, e.g., in [37, 44], have only been answered recently. However, many interesting questions

are still open, including effective dynamics for walls and vortices, as well as their interaction; reduced, effective models which are valid for different relevant parameter regimes; the blow-up behavior of the Landau–Lifshitz and LLG equations; and efficient numerical strategies which reliably handle nonconvexity and nonlocal constraints imposed on weak solutions—to name only a few interesting topics. The following list is mainly motivated by the interests of the authors:

- Understand the relationship between the original Landau–Lifshitz energy and a newly derived finite-temperature version of the micromagnetic energy derived in [59, 60]. Is it computationally feasible to model various domain walls by the stochastic model?
- Develop a microscopic model describing dissipation effects in a physically more reliable way, which could also be used to rigorously derive mesoscopic evolutionary limiting problems.
- Study more complex electromagnetic models describing, e.g., reading and writing of information on a hard disk [103] from modeling, analytical, and numerical viewpoints.
- Clarify the relationship between mesoscopic evolutionary models and Preisach models that have been used in hysteresis computation for many decades. Does the energetic formulation correspond to a Preisach operator? As a starting point, one can study whether the energetic formulation allows for the so-called return-point property. See [107] for details.
- Set valuable benchmarks for the hysteresis calculations and test mesoscopic models for engineering problems.

**Acknowledgments.** We thank S. Bartels (HU Berlin) for providing us with the numerical results from Figure 3.1. The paper was partly written during M.K.'s stay at the Forschungsinstitut für Mathematik of ETH Zurich in May 2004 and A.P.'s stay at ÚTIA AV ČR in Prague in September 2004. The hospitality of the hosting institutes is gratefully acknowledged.

## REFERENCES

[1] A. Aharoni, *Introduction to the Theory of Ferromagnetism*, Oxford University Press, Oxford, 1996.

[2] F. Alouges, *A new algorithm for computing liquid crystal stable configurations: The harmonic mapping case*, SIAM J. Numer. Anal., 34 (1997), pp. 1708–1726.

[3] F. Alouges, S. Conti, A. DeSimone, and Y. Pokern, *Energetics and switching of quasi-uniform states in small ferromagnetic particles*, M2AN Math. Model. Numer. Anal., 38 (2004), pp. 235–248.

[4] F. Alouges and P. Jaisson, *Convergence of a finite element discretization for the Landau-Lifshitz equations*, Math. Model Appl. Sci., 16 (2006), pp. 299–316.

[5] F. Alouges and A. Soyeur, *On global weak solutions for Landau-Lifshitz equations: Existence and nonuniqueness*, Nonlinear Anal., 18 (1992), pp. 1071–1084.

[6] F. Alouges, T. Rivière, and S. Serfaty, *Néel and cross-tie wall energies for planar micromagnetic configurations*, ESAIM Control Optim. Calc. Var., 8 (2002), pp. 31–68.

[7] G. Anzellotti, S. Baldo, and A. Visintin, *Asymptotic behavior of the Landau-Lifshitz model of ferromagnetism*, Appl. Math. Optim., 23 (1991), pp. 171–192.

[8] S. Bartels, *Stability and convergence of finite-element approximation schemes for harmonic maps*, SIAM J. Numer. Anal., 43 (2005), pp. 220–238.

[9] S. Bartels, J. Ko, and A. Prohl, *Numerical approximation of the Landau-Lifshitz-Gilbert equation and finite time blow up of weak solutions*, submitted.

[10] S. Bartels and A. Prohl, *Convergence of an implicit discretization of the Landau–Lifshitz–Gilbert equation*, SIAM J. Numer. Anal., to appear.

[11] S. Bartels and A. Prohl, *Fully practical, constraint preserving, implicit approximation of harmonic map heat flow into spheres*, submitted.

[12] A. Bergqvist, *Magnetic vector hysteresis model with dry friction-like pinning*, Phys. B, 233 (1997), pp. 342–347.
[13] H.A.M. van den Berg, *Self-consistent domain theory in soft ferromagnetic media. II. Basic domain structures in thin film objects*, J. Appl. Phys., 60 (1986), pp. 1104–1113.
[14] G. Bertotti, *Hysteresis in Magnetism*, Academic Press, San Diego, 1998.
[15] M. Bertsch, P. Podio-Guidugli, and V. Valente, *On the dynamics of deformable ferromagnets. I. Global weak solutions for soft ferromagnets at rest*, Ann. Mat. Pura Appl. (4), 179 (2001), pp. 331–360.
[16] M. Brokate and J. Sprekels, *Hysteresis and Phase Transitions*, Springer, New York, 1996.
[17] P. Bryant and H. Suhl, *Thin-film magnetic patterns in an external field*, Appl. Phys. Lett., 54 (1989), pp. 2224–2226.
[18] W.F. Brown, Jr., *Magnetostatic principles in ferromagnetism*, Springer, New York, 1966.
[19] C. Carstensen, S.A. Funken, and A. Prohl, *Stable finite elements in relaxed micromagnetic problems*, in Proceedings of the 16th IMACS World Congress, 2000.
[20] C. Carstensen and D. Praetorius, *Effective simulation of a macroscopic model for stationary micromagnetics*, Comput. Methods Appl. Mech. Engrg., 194 (2005), pp. 531–548.
[21] C. Carstensen and A. Prohl, *Numerical analysis of relaxed micromagnetics by penalised finite elements*, Numer. Math., 90 (2001), pp. 65–99.
[22] C. Carstensen and T. Roubíček, *Numerical approximation of Young measures in non-convex variational problems*, Numer. Math., 84 (2000), pp. 395–415.
[23] M.M. Cerimele, F. Pistella, and V. Valente, *A numerical study of a nonlinear system arising in modeling of ferromagnets*, Nonlinear Anal., 47 (2001), pp. 3357–3367.
[24] N.H. Chang, J. Shatah, and K. Uhlenbeck, *Schrödinger maps*, Comm. Pure Appl. Math., 53 (2000), pp. 590–602.
[25] Y. Chen, S. Ding, and B. Guo, *Partial regularity for two-dimensional Landau-Lifshitz equations*, Acta Math. Sinica, 14 (1998), pp. 423–432.
[26] S. Chikazumi, *Physics of Magnetism*, Wiley, New York, 1964.
[27] R. Choksi and R.V. Kohn, *Bounds on the micromagnetic energy of a uniaxial ferromagnet*, Comm. Pure Appl. Math., 51 (1999), pp. 259–289.
[28] R. Choksi, R.V. Kohn, and F. Otto, *Domain branching in uniaxial ferromagnets: A scaling law for the minimum energy*, Comm. Math. Phys., 201 (1999), pp. 61–79.
[29] J. Cimrák and M. Slodička, *An iterative approximation scheme for the Landau-Lifshitz-Gilbert equation*, J. Comput. Appl. Math., 169 (2004), pp. 17–32.
[30] J. Cimrák, *Error estimates for a semi-implicit numerical scheme solving the Landau-Lifshitz equation with an exchange field*, IMA J. Numer. Anal., 25 (2005), pp. 611–634.
[31] R. Cohen, R. Hardt, D. Kinderlehrer, S.-Y. Lin, and M. Luskin, *Minimum energy configurations for liquid crystals: Computational results*, in Theory and Applications of Liquid Crystals, IMA Vol. Math. Appl. 5, Springer, New York, 1987, pp. 99–122.
[32] R. Cohen, S.-Y. Lin, and M. Luskin, *Relaxation and gradient methods for molecular orientation in liquid crystals*, Comput. Phys. Comm., 53 (1989), pp. 455–465.
[33] J. Coron, *Nonuniqueness for the heat flow of harmonic maps*, Ann. Inst. H. Poincaré Anal. Non Linéaire, 7 (1990), pp. 335–344.
[34] R.P. Cowburn, *The attractions of magnetism for nanoscale data storage*, Philos. Trans. R. Soc. Lond. Ser. A, 358 (2000), pp. 281–301.
[35] E. Dean, R. Glowinski, and C.H. Li, *Applications of operator splitting methods to the numerical solution of nonlinear problems in continuum mechanics and physics*, in Mathematics Applied to Science, Academic Press, New York, 1988, pp. 13–64.
[36] A. DeSimone, *Energy minimizers for large ferromagnetic bodies*, Arch. Ration. Mech. Anal., 125 (1993), pp. 99–143.
[37] A. DeSimone, R.V. Kohn, S. Müller, and F. Otto, *Magnetic microstructures—A paradigm of multiscale problems*, ICIAM 99 (Edinburgh), Oxford University Press, Oxford, 2000, pp. 175–190.
[38] A. DeSimone, R.V. Kohn, S. Müller, and F. Otto, *A reduced theory for thin-film micromagnetics*, Comm. Pure Appl. Math., 55 (2002), pp. 1408–1460.
[39] A. DeSimone, R.V. Kohn, S. Müller, and F. Otto, *Repulsive interaction of Néel walls, and the internal length scale of the cross-tie walls*, Multiscale Model. Simul., 1 (2003), pp. 57–104.
[40] A. DeSimone, R.V. Kohn, S. Müller, F. Otto, and R. Schäfer, *Two-dimensional modeling of soft ferromagnetic films*, R. Soc. Lond. Proc. Ser. A Math. Phys. Eng. Sci., 457 (2001), pp. 2983–2991.
[41] A. DeSimone, H. Knüpfer, and F. Otto, 2-*D Stability of the Néel Wall*, preprint, 2004.
[42] S. Ding and B. Guo, *Initial-boundary value problem for higher-dimensional Landau-Lifshitz systems*, Appl. Anal., 83 (2003), pp. 673–697.

[43] W. E and X.-P. Wang, *Numerical methods for the Landau–Lifshitz equation*, SIAM J. Numer. Anal., 38 (2000), pp. 1647–1665.
[44] W. E, *Selected problems in material science*, in Mathematics Unlimited—2001 and Beyond, Springer, Berlin, 2001, pp. 407–432.
[45] X. Feng and A. Prohl, *Numerical analysis of the Allen-Cahn equation and approximation for mean curvature flows*, Numer. Math., 94 (2003), pp. 33–65.
[46] J. Fidler and T. Schrefl, *Micromagnetic modelling—The current state of the art*, J. Phys. D, 33 (2000), pp. R135–R156.
[47] S. A. Funken and A. Prohl, *Stabilization methods in relaxed micromagnetism*, M2AN Math. Model. Numer. Anal., 39 (2005), pp. 995–1017.
[48] C.J. García-Cervera and W. E, *Effective dynamics for ferromagnetic thin films*, J. Appl. Phys., 90 (2001), pp. 370–374.
[49] T.L. Gilbert, *A Lagrangian formulation of the gyromagnetic equation of the magnetization field*, Phys. Rev., 100 (1955), p. 1243.
[50] B. Guo and M.-C. Hong, *The Landau-Lifshitz equation of the ferromagnetic spin chain and harmonic maps*, Calc. Var., 1 (1993), pp. 311–334.
[51] B. Guo and F. Su, *Global weak solution for the Landau-Lifshitz-Maxwell equation in three space dimensions*, J. Math. Anal. Appl., 211 (1997), pp. 326–346.
[52] B. Guo and F. Su, *The global smooth solution for Landau-Lifshitz-Maxwell equation without dissipation*, J. Partial Differential Equations, 11 (1998), pp. 193–208.
[53] S. Gustafson and J. Shatah, *The stability of localized solutions of Landau-Lifshitz equations*, Comm. Pure Appl. Math., 55 (2002), pp. 1136–1159.
[54] P. Harpes, *Uniqueness and bubbling of the 2-dimensional Landau-Lifshitz flow*, Calc. Var., 20 (2004), pp. 213–229.
[55] A. Hubert and R. Schäfer, *Magnetic Domains*, Springer, Berlin, 1998.
[56] R.D. James and D. Kinderlehrer, *Frustration in ferromagnetic materials*, Contin. Mech. Thermodyn., 2 (1990), pp. 215–239.
[57] P. Joly, A. Komech, and O. Vacus, *On transitions to stationary states in a Maxwell–Landau–Lifshitz–Gilbert system*, SIAM J. Math. Anal., 31 (1999), pp. 346–374.
[58] P. Joly and O. Vacus, *Mathematical and numerical studies of nonlinear ferromagnetic materials*, M2AN Math. Model. Numer. Anal., 33 (1999), pp. 593–626.
[59] M.A. Katsoulakis and P. Plecháč, *Statistical Equilibrium Measures in Micromagnetics*, preprint arXiv:cond-mat/0111319, available online from http://arxiv.org/abs/cond-mat/0111319.
[60] M.A. Katsoulakis, P. Plecháč, and D.K. Tsagkarogiannis, *Mesoscopic modeling for continuous spin lattice systems: Model problems and micromagnetics applications*, J. Stat. Phys., 119 (2005), pp. 347–389.
[61] C.E. Kenig, G. Ponce, and L. Vega, *Small solutions to nonlinear Schrödinger equations*, Ann. Inst. H. Poincaré Anal. Non Linéaire, 10 (1993), pp. 255–288.
[62] J. Ko, *Partially Regular and Singular Solutions to the Landau-Lifshitz (Gilbert) Equations*, Ph.D. thesis, New York University, 2004.
[63] M. Kočvara, M. Kružík, and J.V. Outrata, *On the Control of an Evolutionary Equilibrium in Micromagnetics*, IMA preprint 2026/2005, University of Minnesota, Minneapolis, 2005.
[64] T.R. Koehler, *Hybrid FEM-BEM method for fast micromagnetic calculations*, Phys. B, 233 (1997), pp. 302–307.
[65] M. Kružík, *Maximum principle based algorithm for hysteresis in micromagnetics*, Adv. Math. Sci. Appl., 13 (2003), pp. 461–485.
[66] M. Kružík, *Variational models for microstructure in shape memory alloys and in micromagnetics and their numerical treatment*, in Communications of the Bexbach Colloquium on Science 2000, Vol. II, Proceedings of the conference held in Bexbach, Germany, 2000, M. Robnik and A. Ruffing, eds., Shaker-Verlag, Aachen, 2003, pp. 20–38.
[67] M. Kružík, *Periodic solution to a hysteresis model in micromagnetics*, J. Convex Anal., 13 (2006), pp. 81–99.
[68] M. Kružík, *Periodicity properties of solutions to a hysteresis model in micromagnetics*, in Numerical Mathematics and Advanced Applications, Proceedings of ENUMATH 2003, M. Feistauer et al., eds., Springer, Berlin, 2004, pp. 605–614.
[69] M. Kružík and A. Prohl, *Young measure approximation in micromagnetics*, Numer. Math., 90 (2001), pp. 291–307.
[70] M. Kružík and A. Prohl, *Macroscopic modeling of magnetic hysteresis*, Adv. Math. Sci. Appl., 14 (2004), pp. 665–681.
[71] M. Kružík and T. Roubíček, *Specimen shape influence on hysteretic response of bulk ferromagnets*, J. Magn. Magn. Mat., 256 (2003), pp. 158–167.

[72] M. Kružík and T. Roubíček, *Interactions between demagnetizing field and minor-loop development in bulk ferromagnets*, J. Magn. Magn. Mat., 277 (2004), pp. 192–200.
[73] L.D. Landau and E.M. Lifshitz, *On the theory of the dispersion of magnetic permeability of ferromagnetic bodies*, Phys. Z. Sowj., 8 (1935), pp. 153–169.
[74] S.-Y. Lin and M. Luskin, *Relaxation methods for liquid crystal problems*, SIAM J. Numer. Anal., 26 (1989), pp. 1310–1326.
[75] M. Luskin and L. Ma, *Analysis of the finite element approximation of microstructure in micromagnetics*, SIAM J. Numer. Anal., 29 (1992), pp. 320–331.
[76] L. Ma, *Analysis and Computation for a Variational Problem in Micromagnetics*, Ph.D. thesis, University of Minnesota, Minneapolis, 1991.
[77] C. Melcher, *The logarithmic tail of Néel walls in thin films*, Arch. Ration. Mech. Anal., 168 (2003), pp. 83–113.
[78] C. Melcher, *Existence of partially regular solutions for Landau-Lifshitz equations in* $\mathbb{R}^3$, Comm. Partial Differential Equations, 30 (2005), pp. 567–587.
[79] A. Mielke, *Energetic formulation of multiplicative elastoplasticity using dissipation distances*, Contin. Mech. Thermodyn., 15 (2003), pp. 351–382.
[80] A. Mielke and F. Theil, *Mathematical model for rate-independent phase transformations*, in Models of Continuum Mechanics in Analysis and Engineering, H.-D. Alber, R. Balean, and R. Farwig, eds., Shaker-Verlag, Aachen, 2001, pp. 117–129.
[81] A. Mielke and F. Theil, *On rate-independent hysteresis models*, Nonlinear Differential Equations Appl., 11 (2004), pp. 151–189.
[82] A. Mielke, F. Theil, and V. Levitas, *A variational formulation of rate-independent phase transformations using extremum principle*, Arch. Ration. Mech. Anal., 162 (2002), pp. 137–177.
[83] P.B. Monk and O. Vacus, *Error estimates for a numerical scheme for ferromagnetic problems*, SIAM J. Numer. Anal., 36 (1999), pp. 696–718.
[84] F. Murat, *Compacité par compensation*, Ann. Scuola Norm. Sup. Pisa Cl. Sci. (4), 5 (1978), pp. 489–507.
[85] P. Pedregal, *Relaxation in ferromagnetism: The rigid case*, J. Nonlinear Sci., 4 (1994), pp. 105–125.
[86] P. Pedregal, *Parametrized Measures and Variational Principles*, Birkhäuser, Basel, 1997.
[87] P. Pedregal, *Numerical computation of parametrized measures*, Numer. Funct. Anal. Optim., 16 (1995), pp. 1049–1066.
[88] F. Pistella and V. Valente, *Numerical stability of a discrete model in the dynamics of ferromagnetic bodies*, Numer. Methods Partial Differential Equations, 15 (1999), pp. 544–557.
[89] P. Podio-Guidugli and V. Valente, *Existence of global-in-time weak solutions to a modified Gilbert equation*, Nonlinear Anal., 47 (2001), pp. 147–158.
[90] P. Podio-Guidugli and G. Tomassetti, *On the evolution of domain walls in hard ferromagnets*, SIAM J. Appl. Math., 64 (2004), pp. 1887–1906.
[91] N. Popović and D. Praetorius, *Application of* $\mathcal{H}$*-matrices in micromagnetics*, Computing, 74 (2005), pp. 177–204.
[92] I. Privorotskii, *Thermodynamic Theory of Domain Structures*, Wiley, New York, 1976.
[93] A. Prohl, *Computational Micromagnetism*, Teubner, Stuttgart, 2001.
[94] T. Roubíček, *Relaxation in Optimization Theory and Variational Calculus*, W. de Gruyter, Berlin, 1997.
[95] T. Roubíček, *Microstructure in ferromagnetics and its steady-state and evolution models*, in Communications of Bexbach Colloquium on Science 2000, II, M. Robnik and A. Ruffing, eds., Shaker-Verlag, Aachen, 2003, pp. 39–52.
[96] T. Roubíček, *Models of microstructure evolution in shape memory alloys*, in Proceedings of the NATO workshop Nonlinear Homogenization and Its Application to Composites, Polycrystals and Smart Materials, P. Ponte Castañeda et al., eds., Kluwer Academic, Dordrecht, The Netherlands, 2004, pp. 269–304.
[97] T. Roubíček and M. Kružík, *Microstructure evolution model in micromagnetics*, Z. Angew. Math. Phys., 55 (2004), pp. 159–182.
[98] T. Roubíček and M. Kružík, *Mesoscopic model for ferromagnets with isotropic hardening*, Z. Angew. Math. Phys., 56 (2005), pp. 107–135.
[99] T. Schrefl, J. Fidler, K.J. Kirk, and J.N. Chapman, *Domain structures and switching mechanisms in patterned magnetic elements*, J. Magn. Magn. Mat., 175 (1997), pp. 193–204.
[100] M. Struwe, *On the evolution of harmonic maps of Riemannian surfaces*, Comment. Math. Helv., 60 (1985), pp. 558–581.

[101] M. Struwe, *Geometric evolution problems*, in Nonlinear Partial Differential Equations in Differential Geometry (Park City, UT, 1992), IAS/Park City Math. Ser. 2, AMS, Providence, RI, 1996, pp. 259–339.
[102] P.L. Sulem, C. Sulem, and C. Bardos, *On the continuous limit for a system of classical spins*, Comm. Math. Phys., 107 (1986), pp. 431–454.
[103] J. Sun, F. Collino, P.B. Monk, and L. Wang, *An eddy-current and micromagnetism model with applications to disk write heads*, Internat. J. Numer. Methods Engrg., 60 (2004), pp. 1673–1698.
[104] L. Tartar, *Compensated compactness and applications to partial differential equations*, in Nonlinear Analysis and Mechanics: Heriot-Watt Symposium, Vol. IV, R. Knops, ed., Res. Notes in Math. 39, Pitman, Boston, London, 1979, pp. 136–212.
[105] C. Truesdell and W. Noll, *The nonlinear field theories in mechanics*, in Encyclopedia of Physics III/3, Springer, Heidelberg, 1965.
[106] A. Visintin, *On Landau-Lifshitz' equations for ferromagnetism*, Japan J. Appl. Math., 2 (1985), pp. 49–84.
[107] A. Visintin, *Differential Models of Hysteresis*, Springer, Berlin, 1994.
[108] A. Visintin, *Modified Landau-Lifshitz equation for ferromagnetism*, Phys. B, 233 (1997), pp. 365–369.
[109] L.R. Walker, *A Treatise on Magnetism, Vol.* III, G.T. Rado and H. Suhl, eds., Academic Press, New York, 1963, pp. 450–453.
[110] X.-P. Wang, C.J. García-Cervera, and W. E, *A Gauss-Seidel projection method for micromagnetics simulations*, J. Comput. Phys., 171 (2001), pp. 357–372.
[111] L.C. Young, *Generalized curves and existence of an attained absolute minimum in the calculus of variations*, C. R. Soc. Lett. Varsovie, Classe III, 30 (1937), pp. 212–234.